

New Horizon in stabilization of single atoms on metal-oxide supports for CO₂ reduction

Muhammad Abbas^a, Muhammad Aurang Zeb Gul Sial^{b,*}

^a Department of Chemistry and Biochemistry, The University of Texas at Dallas, 800 West Campbell Road, Richardson, TX, 75080, USA

^b Multi-scale Porous Materials Centre, Institute of Advanced Interdisciplinary Studies, School of Chemistry and Chemical Engineering, Chongqing University, Chongqing, 400044, PR China

ARTICLE INFO

Keywords:

Single atoms
Metal-oxides support
CO₂ reduction

ABSTRACT

Electrochemical CO₂ reduction is a promising route to convert CO₂ into the value added chemicals, and to control the increasing accumulation of CO₂ in the atmosphere. The CO₂ molecule is stable and chemically inert, so a highly efficient electrocatalyst is required for CO₂ reduction. The single atoms with metal oxide support is a new frontier in CO₂ reduction. The supported single atoms contain disperse isolated atoms with an appropriate support maximize the atom efficiency of metals for boosting the catalytic performance. In this review, we had discussed state-of-the-art research on the synthesis of single atoms supported on the metal oxide for boosting catalytic activity for CO₂ reduction and special emphasis is placed on the influence of single atoms supported on metal oxide on the CO₂ reduction. Furthermore, we had discussed the challenges, and opportunities for paving the development of single atoms with metal support and their application in electrocatalytic CO₂ reduction.

1. Introduction

The excessive consumption of fossil fuels for industrial and economic development in the past few decades has produced serious environmental problems [1–5]. Among these issues, the increased concentration of CO₂ in the atmosphere is a severe threat to the globe [6–8]. Excessive CO₂ emissions contribute to the greenhouse effect, which is the key cause of global warming and climate change [9–11]. Thus, there is an urgent need to develop effective technologies to keep global carbon net emissions within an acceptable range [12,13]. Among many possible alternatives to maintain the global CO₂ balance, such as decarbonization, carbon sequestration, carbon recycling, and electrochemical CO₂ reduction (ECR): The ECR approach offers a potentially sustainable approach to depressing CO₂ concentration and converting it into fuels and chemicals (Fig. 1) [9]. However, the ECR is kinetically sluggish because CO₂ is a linear molecule, thermodynamically stable, and chemically inert. A highly active catalyst is required for speeding up CO₂ reduction [14,15] (see Table 1).

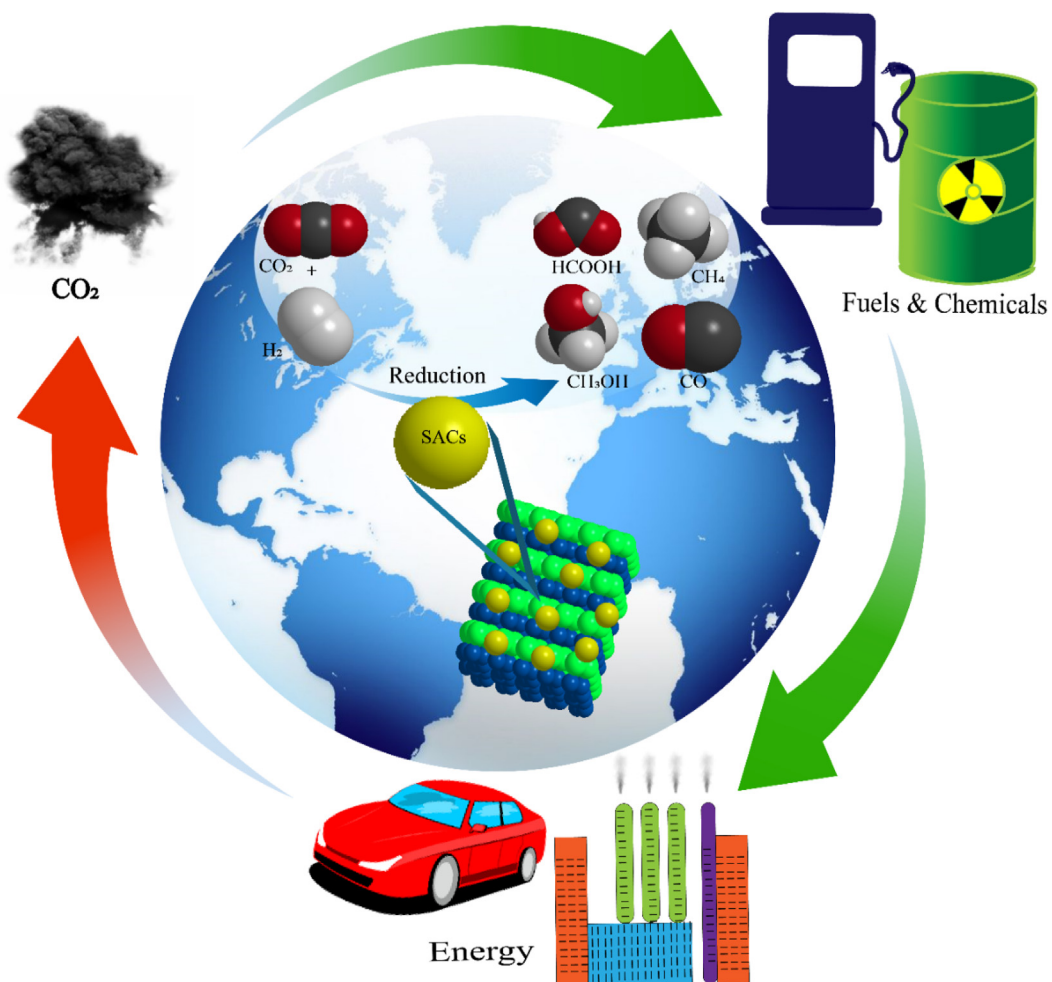
Single atom catalysts (SACs) have attracted attention in the past few years for catalytic applications due to their particular behavior and maximum atom efficiency [16,17]. Single atoms reveal that phase interfaces with spatial atomic isolation may endow unexpected properties as compared to nanoparticles (NPs) [17–19]. Furthermore, due to high

surface energy, single-atoms form clusters or nanoparticles via agglomeration or sintering. To avoid this, they are normally prepared using low concentrations of loading atoms to prevent the agglomeration of single atoms [20]. However, it is a big challenge to improve the loading concentration of single atoms for practical applications [21]. To overcome these issues, single atoms are prepared on the metal oxide supports. This concept was first introduced by Tausig et al., in 1978; he showed the hydrogen and carbon monoxide sorption capacity of noble metal supported on TiO₂ oxide [22]. The interactions of single atoms and metal support stabilize single atoms leading to exceptionally high activity for various catalytic applications. This is due to the d-band center of metal sites that can be changed as a result of electronic perturbation of support [23–26]. The metal chemical state change by charge transfer from interface and plays an important role to activate the reactant. However, the understanding of single atoms with metal support for electrocatalytic properties is still infancy because of the inevitable interface of intrinsic metal effects [27,28].

To design nanostructured catalysts and optimize their catalytic properties, various synthetic methodologies and advanced characterization techniques have been developed. Furthermore, the studies of structural effect on the catalytic efficiency at atomic level have also been reported. The high-quality review articles about single atoms with metal oxide support for CO₂ reduction are reported, whereas the concept of the

* Corresponding author.

E-mail address: zeb@cqu.edu.cn (M.A.Z.G. Sial).

Fig. 1. Schematic Presentation of CO₂ reduction and its uses.**Table 1**Comparison of CO₂RR of different Catalysts.

SACs	Support	Major Product	Other Products	Synthesis strategy/conditions	References
Ag	CeO ₂ -ZnO	CH ₄ 95%	CO and CH ₄ 377.75 and ~20.12 μmol g ⁻¹	Hydrothermal, 60 °C, 6 h	[71]
Pt	CeO ₂ NPs	CO 100%	–	Wetness impregnation followed by sol-gel, 42h	[17]
Pd	Perovskite	CO	–	Hydrothermal method and co-precipitation, 27h	[57]
Cu	CeO ₂ nanorods	CH ₄ 68% FE _{CH4}	CH ₄ , C ₂ H ₄ , H ₂	hydrothermal, Cu doping, 250 °C, 2h	[56]
Ir	α-Co(OH) ₂	CO 97.6% FE	–	Wetness impregnation	[67]

design of single atoms on metal oxide support has not been clear and needs much more attention [8,29–31]. In this review, we attempt to address the synthesis strategies of single atoms with metal oxide support in detail. High catalytic performance for CO₂ reduction from support and single atoms is elaborated with respect to surface/catalyst support interaction. Finally, opportunities and challenges are also suggested for the synthesis of single atoms with support for future development.

2. Synthesis of single atoms with metal supports

The high surface energy of single metal atoms tends to agglomerate atoms into clusters or nanoparticles. One of the most convenient approaches to synthesize single atoms catalyst is to prevent agglomeration of metal species, preserving adequate distance between molecules of the metal precursor. In this regard, single metal atoms are grown on different

supports. Selecting suitable support and controlling the metal loading content plays a vital role in the formation of single atoms as metal supported catalysts. The different types of support are used for stabilization of single atoms, for example, carbon support, N-doped carbon support, carbon nanotubes supported single atoms, but among various types of supported single atoms catalysts (SACs), those based on oxide supports have attracted particular attention. The oxides exhibit specific and variable properties such as surface acidity/basicity and redox features (especially when reducible metals are involved), which lead to specific catalytic properties. Moreover, the oxide materials have abundant defective sites (steps, corners, vacancies) on their surface and due to the presence of –OH groups on the surface can also serve as the anchoring sites for single metal atoms. The single atoms with metal oxide support greatly influence the catalytic properties due to synergistic effects. The robustness of oxides at elevated temperatures is also an important

starting point for enhancing the mechanical and thermal stability of SACs. Taken together, oxide-supported SACs exhibited superior performance as compared to the carbon support and other support in catalytic applications. For the synthesis of single atoms with metal oxide support, the location of single atom should be related to the structure of the support. A model rutile support surface (110) provide three different types of anchoring sites of single atoms, e.g., metal sites, oxygen vacancy and through metal oxygen bonding. Furthermore, the support stabilizes the single atoms and prevent from sintering during the electrocatalysis [32]. The single atoms on metal support are often prepared by coprecipitation and impregnation methods. The ratio of loading metal and metal support plays a vital role for the growth of single atoms without agglomeration [16].

2.1. Synthesis of single Pt atoms on metal oxide supports

Zhang et al. prepared single atoms with metal support catalyst by coprecipitation method with a low metal loading. They used chloroplatinic acid ($H_2PtCl_6 \cdot 6H_2O$) and ferric nitrate ($Fe(NO_3)_3 \cdot 9H_2O$) aqueous solution as precursors of platinum (Pt) and iron oxide as support ($FeOx$). Both aqueous solutions of Pt/Fe were mixed with an atomic ratio of 1:1430. The solid precipitates were obtained by adjusting the pH to 8 by adding sodium carbonate (Na_2CO_3). The obtained solid was dried and calcined at high temperature. The loading amount of Pt was 0.17 wt% measured by inductively coupled plasma spectroscopy (ICP). The single Pt atom in the Pt/ $FeOx$ catalyst was observed by the aberration-corrected high angle annular dark field scanning electron microscope (AC HAADF-STEM). The X-ray absorption fine structure (XAFS) revealed that Pt single atom is bonded with the oxygen atom of $FeOx$ support to form Pt–O coordination. The low loading content of platinum played a vital role in the formation of single Pt atoms. By increasing the Pt:Fe atomic ratio to 1:95 to give the 2.5 wt % Pt loading, Pt nanoparticles were observed instead of single atoms. This single Pt atom has a high carbon monoxide (CO) oxidation activity because it lowers the energy of CO adsorption and activation barrier [33]. Zhang et al. also reported the synthesis of high loading single Pt atom with Fe_2O_3 support via atom vaporization method. The Pt single atom is fixed on the metal oxide support by forming strong covalent bonds. Pt single atoms on Fe_2O_3 support were prepared by the coprecipitation method. The chloroplatinic acid ($H_2PtCl_6 \cdot 6H_2O$) and ferric nitrate ($Fe(NO_3)_3 \cdot 9H_2O$) aqueous solution were mixed with Na_2CO_3 at 50 °C with constant stirring and aged for 2 h. The resultant solid was washed with deionized water, dried in an oven and calcined at 800 °C to get Pt single atom with Fe_2O_3 support. The loading of Pt was determined by ICP. Furthermore, they also studied the effect of concentration of Pt on Fe_2O_3 support, while increasing the concentration of Pt up to 2 wt %, Pt clusters are formed instead of Pt single atoms. In the synthesis of a single Pt atom, temperature, and atmosphere often play an important role, frequently calcinating at 600 °C in air, resulting in the formation of smaller Pt particles. While calcination in argon, large Pt particles were formed. Furthermore, an oxidizing environment is necessary for the formation of single Pt atoms, because Pt nanoparticles liberate PtO_2 at an elevated temperature that is trapped by large Pt nanoparticles (Ostwald ripening) or on a unique oxide site. Due to the strong interaction between Pt and Fe_2O_3 support, Pt atoms vaporized were trapped and stabilized by Fe_2O_3 support. The EXAFS spectrum also confirmed that Pt was dispersed in atomic form [34]. The catalytic behavior of Pt mainly depends on the size of Pt NPs. Recently, Lu et al. reported the synthesis of single Pt atoms supported on the iron-chromium oxide composite. First, they prepared the iron-chromium oxide composite by the sol-gel method. $Cr(NO_3)_3 \cdot 9H_2O$, $Fe(NO_3)_3 \cdot 9H_2O$, and citric acid were dissolved in deionized water. The viscous gel was obtained by heating the mixture solution at 90 °C. The gel was dried at 120 °C and calcined at 500 °C. The Pt single atoms supported on the iron-chromium oxide support were synthesized by the wet impregnation method. The aqueous Pt (NO_3)₂ solution was immersed on iron chromium oxide support or gel. After keeping the suspension at room temperature for 3 h,

water was evaporated at 90 °C and dried at 100 °C. The single Pt atoms were obtained on iron chromium oxide support by calcination at 300 °C. The XRD patterns show identical diffractions with and without Pt, indicating that Pt is atomically dispersed. However, the XRD diffraction patterns of Pt particles are observed for the high loading of Pt. The AC HAADF STEM confirmed that Pt is present in the form of single atoms in a low loading; no aggregation of Pt atoms was observed, indicating that Pt atoms are stable under reduction temperature [35].

Li et al. reported the synthesis of a high concentration of single Pt atoms supported on CuS hollow support by the novel ion-exchange method. The interaction between Pt and the support is the key to synthesize single Pt atoms. It controls the kinetics and prevents the formation of Pt–Pt bonding due to the close interaction between Pt and support. Li et al. prepared CuS nanoparticles by mixing $Cu(CH_3COO)_2$ in the solution of 1-dodecanethiol and 1-dodecanol. The mixture was heated under constant stirring for 20 min under argon flow at 230 °C. The product was precipitated by adding ethanol and cyclohexane mixture. The obtained product was redispersed in cyclohexane. Cyclohexane dispersion of CuS was used as a precursor of support. For the synthesis of single Pt atoms, $H_2PtCl_6 \cdot 6H_2O$ solution in ethylene glycol was added to CuS cyclohexane dispersion and degassed by Ar bubbling at 100 °C and further heated at 180 °C for 5 min. Later, the reaction mixture was cooled to 80 °C and ethanol was injected. The single Pt atom supported on the CuS sphere was obtained by cooling till 50 °C and exposed to air for 45 min. The TEM images show the hollow nature of spheres with rough surface (Fig. 2 b). The powder XRD, HRTEM, and selected area electron diffraction (SAED) confirmed the amorphous nature of sample (Fig. 2). The elemental distribution confirmed the presence of Pt, Cu and S. The AC HAADF-STEM confirmed the isolated nature of Pt species, as shown in Fig. 2f [36].

Li et al. reported the synthesis of Pt single atoms supported on the defect-rich $Ni(OH)$ nanoboards (NBs) by a simple wet impregnation method. First, they synthesized polycrystalline $Ni(OH)x$ NBs by the wet chemical method on a large scale. In detail, $Ni(NO_3)_3$ was dissolved in deionized water and triethylene glycol, and then mixed with an aqueous solution of tetrabutylammonium hydroxide (TBAH), Urea, and $NaHCO_3$. After stirring at room temperature, the above mixture was transferred to an autoclave and heated at 120 °C for 12 h. The product was obtained by centrifugation, washing with ethanol, and drying in an oven. The $Ni(OH)x$ NBs as-synthesized were used as support to allow the adsorption of Pt atoms for the growth of single Pt atoms and NBs. The obtained $Ni(OH)x$ NBs were first ultrasonically dispersed in ethanol, and H_2PtCl_6 solution in ethanol was added dropwise in the NBs solution with continuous stirring; the mixture was stirred overnight and the suspension was centrifuged. The recovered solid was dried and reduced in 5% H_2/N_2 at 100 °C for 2 h. The TEM image confirmed that the NBs display uniform morphology. STEM revealed that Pt particles are not formed on NBs. The EDS mapping confirmed that Pt is evenly distributed in NBs. AC HAADF STEM has confirmed that Pt exists in the form of single independent species. The EXAFS spectrum confirmed that Pt–Ni contribution is weak as compared to Pt–O and Pt did not form Pt–Pt bonding. The EXAFS spectrum also confirm that Pt is present in the form of isolated single atoms on $Ni(OH)x$ NBs. The abundant vacancy defects on the surface of $Ni(OH)x$ play a crucial role for stabilizing single Pt atoms with 2.3 wt% and no aggregation of platinum particles is observed [37].

Strong metal-support interaction (SMSI) or atomically dispersed atoms on various supports has gained a great attraction due to their unique catalytic properties. Single atoms catalysts eliminate the geometry and size effect and provide a simple model system to study active centers and their chemical states for catalysis. The interaction between single atoms and support plays a critical role in catalysis as compared to nanoparticles and support. Recently, Zhang et al. reported the synthesis of single Pt atoms on TiO_2 support and Pt NPs on TiO_2 support. First, they prepared a metastable phase of TiO_2 nanosheets (NSs) by hydrothermal method with a high surface area. Pt with 1% loading was deposited on nanosheets by a photochemical method and protection agent was

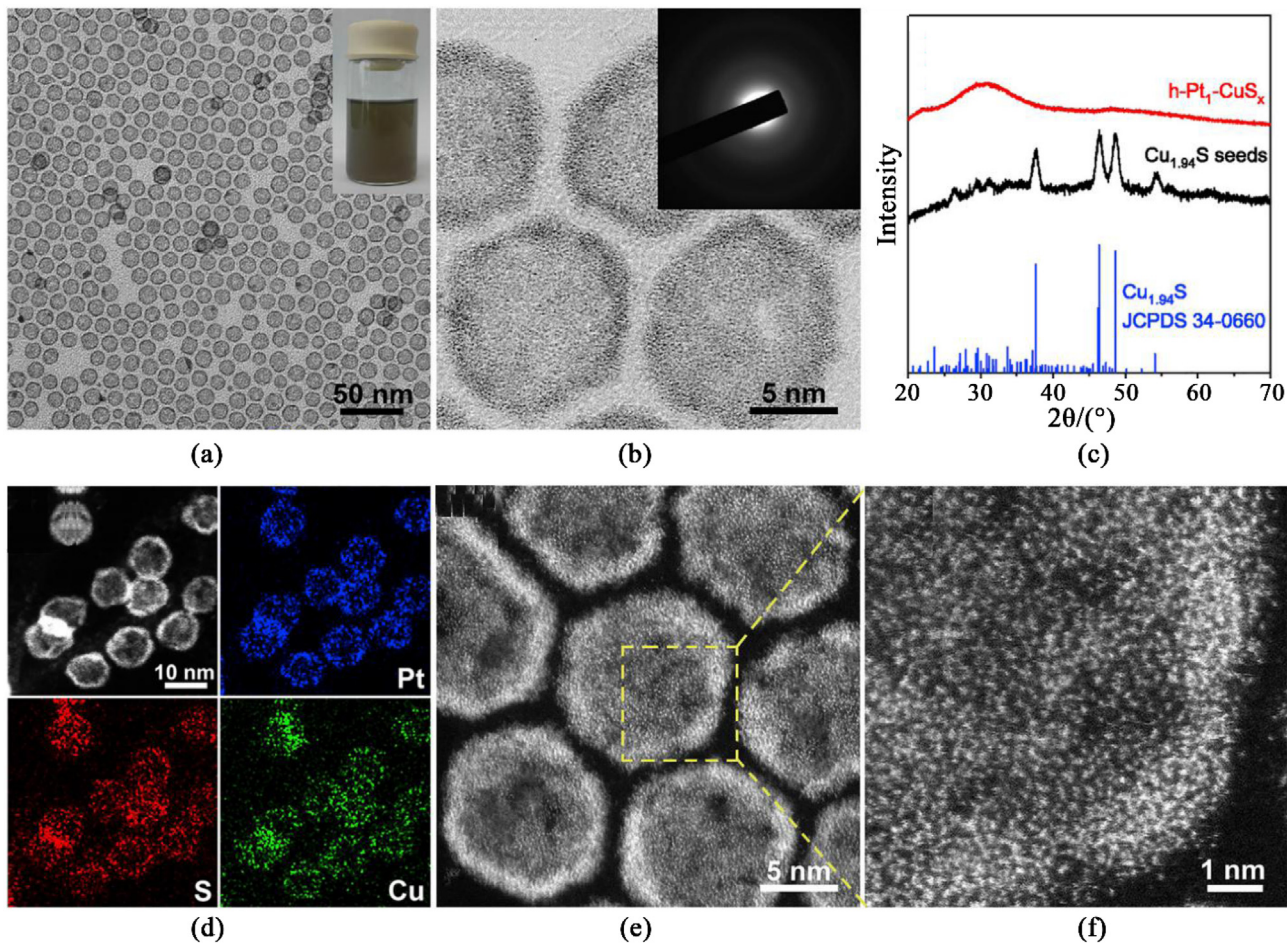


Fig. 2. Characterizations of h-Pt₁-CuS_x Nanoparticles (a) TEM image of h-Pt₁-CuS_x. Inset is the photograph of the nanoparticles dispersed in cyclohexane. (b) High-magnification TEM image. Inset is the SAED pattern. (c) XRD pattern of the Cu_{1.94}S nanoparticle seeds and the h-Pt₁-CuS_x nanoparticles. (d) EDS elemental mapping of Pt, S, and Cu. (e and f) AC-HAADF-STEM images of h-Pt₁-CuS_x [36].

removed by calcination at 350 °C. The actual loading amount of Pt was 0.77 wt% measured by ICP-OES. The XRD pattern suggested that no Pt phase was detected and Pt was present in the form of dispersion. The AC HAADF STEM characterization at low magnification confirmed that Pt single atoms were distributed on TiO₂ NSs [38].

Gao et al. reported the synthesis of single Pt atoms anchored on titania nanowires array or integrated on honeycomb substrate. This unique catalyst offers a remarkable high oxidation activity for CO oxidation and retains its morphology. First, they grew mesoporous rutile TiO₂ onto channel surface of cordierite honeycombs. The loading amount of TiO₂ was measured by ICP-MS. The rutile nanoarrays of TiO₂ are arranged in the form of bundles of individual nanowires of TiO₂ that were grown on the substrate. The prepared rutile TiO₂ nanoarrays have high surface area with a mesoporous structure. The Pt was loaded onto nanowires by dip-coating method. AC HAADF-STEM was used to investigate the distribution of Pt on TiO₂. The AC HAADF-STEM clearly revealing that Pt is well dispersed on the TiO₂ surface. The Pt dispersion was measured by H₂ chemisorption and it confirmed that Pt is dominantly dispersed in atomic form. Furthermore, they prepared nanowires with different porosities by changing the calcination temperature to study the influence of Pt single atoms loading. Pt particles have not been observed by using different ratio of TiO₂ and Pt single atom retain on porous nanowires in the form of single atoms that suggest the excellent thermal stability of Pt single atoms at TiO₂ nanowires (Fig. 3d) [39].

Zhang et al. reported the synthesis of single Pt atoms on nanoporous TiO₂ films with exposed (001) facet by immersion and reduction method as presented in the schematic diagram (Fig. 4a). For the growth of single

atom on TiO₂ nanosheets (NSs), the TiO₂ nanosheets were pretreated with NaOH and immersed in aqueous solution of H₂PtCl₆. The mixture was stirred for 3 h and aged for 1 h and dried in vacuum oven. The single atoms of Pt grown on TiO₂ NSs were obtained by reduction in H₂/He mixture. The prepared TiO₂ NSs have primary anatase and rutile phase as well as confirmed by XRD pattern. The Pt peaks were not observed and crystal phase of TiO₂ NSs remains the same after Pt implantation. The Pt single atoms with different concentrations of Pt were implanted and the amount was measured by ICP-MS. By increasing the concentration of implanting Pt, the intensity of (101) plane of anatase gradually decrease because mostly Pt is implanted on the nanopores of TiO₂ NSs. The FESEM image of TiO₂ NSs shows that the NSs have flat and square top surface (Fig. 4b). The Pt NPs (white dots) could be clearly observed in a spherical shape in the high loading sample while no Pt particles were observed in the low loading sample. The HRTEM image also confirmed the presence of anatase phase. HRTEM of the high loading Pt-TiO₂ NSs shows small Pt spheres or cluster also. Fig. 4g clearly indicated that Pt is present in the low loading sample in the form of isolated species [40].

Li et al. reported the synthesis of single Pt atoms assisted by the defective TiO₂ support. The single Pt atoms not only serve as proton reduction sites but promote TiO₂ units to generate surface oxygen vacancies via a hydrogen spillover effect. It helps to establish an atomic interface between single Pt atoms and a Ti³⁺ defect with an active core of atomically dispersed Pt–O–Ti³⁺. The synthesis of single Pt atoms is shown in a schematic diagram (Fig. 5 a). First, they prepared sodium titanate that displays a multilayer tubular morphology. The precursor of Pt, H₂PtCl₆·6H₂O in 0.1 M HCl aqueous solution is added in sodium

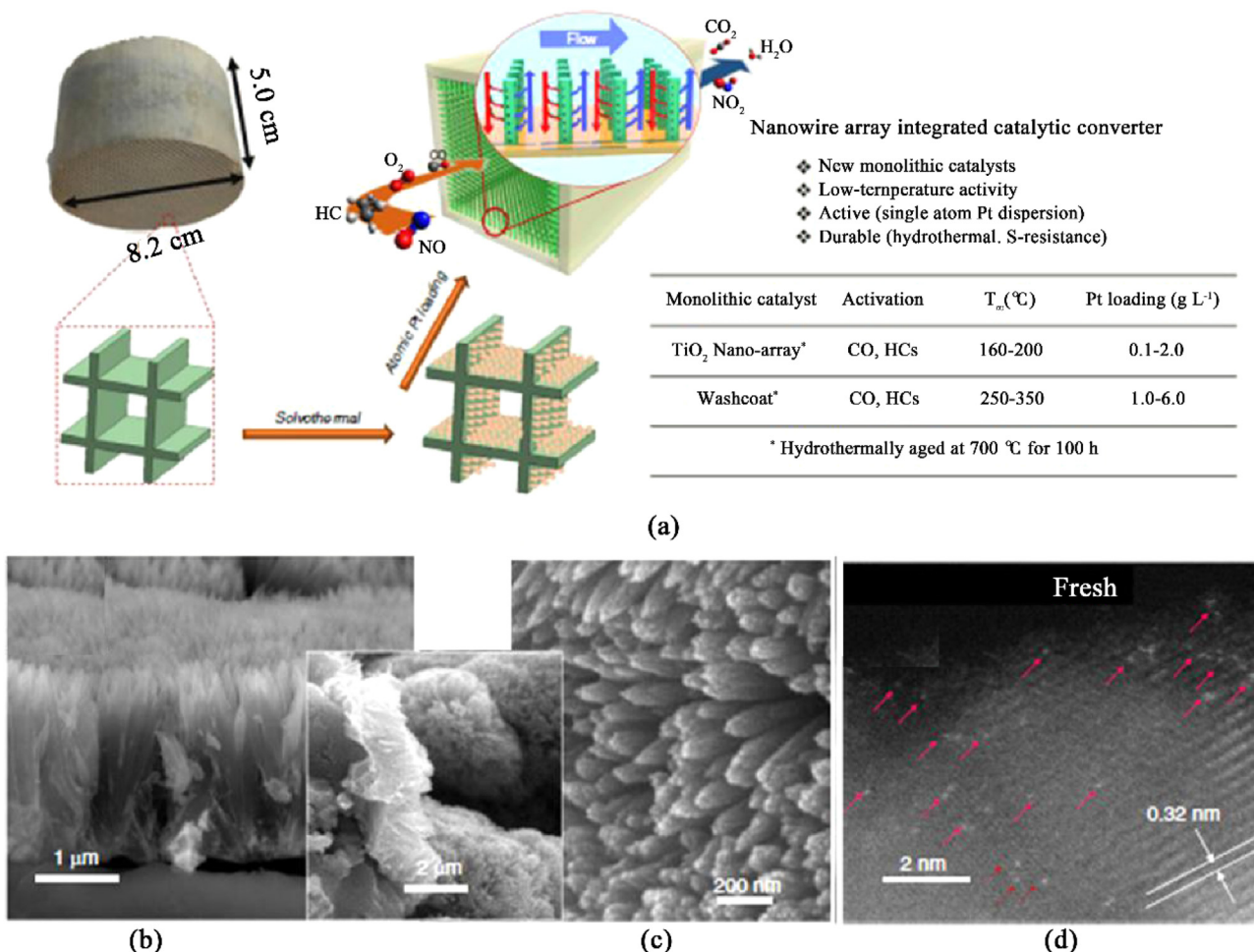


Fig. 3. Synthesis and structure of single Pt atoms supported on rutile TiO₂ nanowire arrays. Schematic illustration of integration process of Pt₁/TiO₂ nanowire array forest onto ceramic monoliths and physicochemical and catalytic characteristics of such DOC catalytic converters (a). Cross-sectional (b) and (c) top view SEM images of rutile TiO₂ NA on a cordierite honeycomb; inset: low-magnification cross-sectional view of cordierite substrate interface with conformably distributed TiO₂ nanowire forest. The AC-HAADF STEM images of Pt₁/TiO₂ NA prepared by microwave-assisted dip-coating (d), the bright dots on the surface of TiO₂ are Pt atoms, as pointed by red arrow-heads [39].

titanate suspension under continuous stirring. The support defective TiO₂ was obtained by drying and calcination at 400 °C. The single Pt atom supported on defective TiO₂ was obtained by a low temperature reduction treatment under 5% H₂/Ar atmospheres at 160 °C. The Pt/defective TiO₂ catalyst has a multilayer tubular morphology with a rough surface. The XRD pattern was well matched with the TiO₂ anatase process and no peak match was observed with the Pt species. The HAADF-STEM image confirms that Pt does not form nanoparticles (Fig. 5 e-f). The EDS reveals the uniform dispersion of Pt, Ti, O elements (Fig. 5 d). The AC HAADF-STEM demonstrates the presence of individuals Pt atoms and ICP-OES confirms the loading of Pt is 0.02 wt% [41].

Narula et al. reported the synthesis of single Pt atoms supported on the Al₂O₃ surface. First, they prepared Al₂O₃ by sol-gel method. In details, alumina powder was added to an aqueous solution of chloroplatinic acid and stirred. The water was gradually evaporated with continuous stirring by heating in an oil bath. The obtained powder was calcined at 450 °C in air. For the synthesis of single Pt atoms, the low loading amount of Pt is important. AC TEM was used to confirm the presence of single Pt atoms in multiple areas. The Pt single atoms present on the surface of Al₂O₃ and they are not embedded on the alumina. Abreaction corrected electron microscopy (ACEM) reveals that mostly Pt atoms are more than 3 Å apart from each other. The X-ray adsorption near edge (XANES) also confirmed that Pt is present isolatedly [42].

Strong interaction between isolated single Pt atoms and support can

tune the electronic structure leading to an improved stability. Luo et al. reported the low-temperature pyrolysis of organic-inorganic hybrid nanorods with a Pt precursor to synthesis Pt single atoms supported on the amorphous MoO_x nanorods. First, they synthesize MoO_x nanorods by hydrothermal method and Pt single atom was adsorbed by wet impregnations method as shown in Fig. 6a. In details, they synthesized (C₂H₁₀N₂)[Mo₃O₁₀] and adsorbed H₂PtCl₆ on its surface. The functional groups O²⁻ and -OH help to electrostatically adsorb metal precursors on the surface of nanorods. The Pt single atoms supported on MoO_x nanorods were obtained by calcination under Ar gas. Ar gas separated the long chain of (C₂H₁₀N₂)[Mo₃O₁₀] carbonized and N doped carbon by calcination and oxygen moieties. The single Pt atoms supported on MoO_x naorods were prepared by low-temperature pyrolysis, which is more practical as compared to traditional synthesis. The SEM image shows that the 1D nanorod structure is well preserved (Fig. 6 b). The HRTEM image confirms the amorphous nature of the sample (Fig. 6 c). The HAADF-STEM image confirms the presence of isolated single Pt atoms and distributed on amorphous MoO_x substrate (Fig. 6 d). Energy dispersive X-ray revealed that Pt Single atoms is uniformly distributed on MoO_x nanorods (Fig. 6 e) [43].

Du et al. reported the synthesis of single Pt atoms supported on MoC-carbon nanofibers (CNF). In details, platinum bis(acetylacetonate) (Pt (acac)₂), phosphomolybdic acid (PMA) were dissolved into DMF and electrospun into polyacrylonitrile (PAN) fibers as shown in schematic

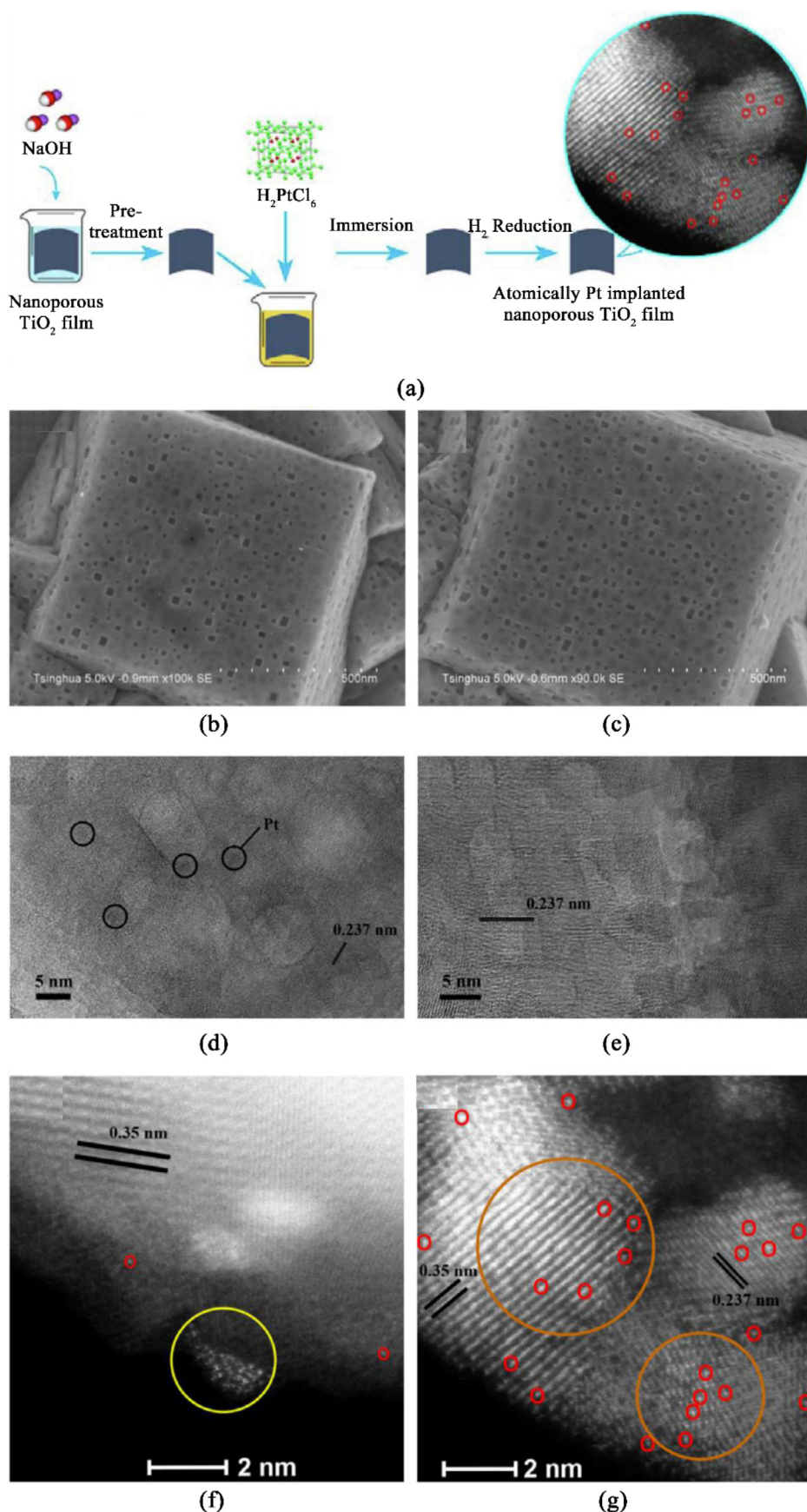


Fig. 4. Schematic illustration of immersion and reduction process combined with the pretreatment of nanoporous TiO_2 film in an NaOH solution for the preparation of atomically Pt implanted nanoporous TiO_2 film with exposed [6] facets (a). FESEM (b, c), HRTEM (d, e) and HAADF-STEM (f, g). The black circle is Pt nanoparticles, the red circle is Pt single atom, the yellow circle is Pt cluster, and the orange circle is nanopore [40].

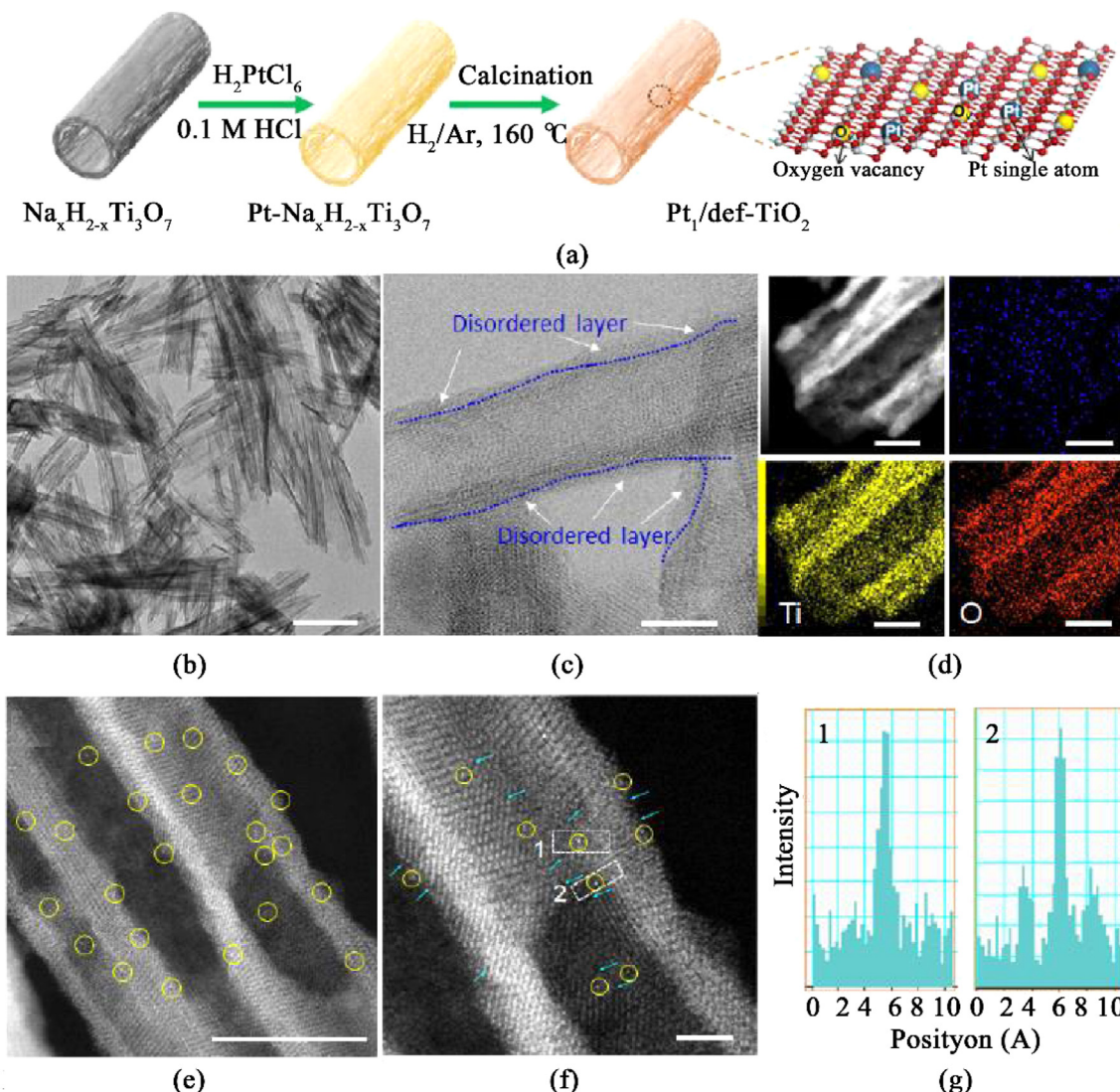


Fig. 5. (a) Schematic diagram of preparation process of the Pt/def-TiO₂ catalyst. TEM image (b), HRTEM image (c), and EDS mappings of Pt (blue), Ti (green), O (red), respectively (d) of Pt₁/def-TiO₂. (e, f) AC HAADFSTEM image (e) and the corresponding enlarged image (f) of Pt/def-TiO₂ catalyst. The Pt atoms are marked by the yellow circles. (g)The intensity profiles obtained in regions 1 and 2 in (f). Scale bars are 100 nm, 5 nm, 10 nm, 10 nm and 2 nm in b, c, d, e and f, respectively [41].

diagram Fig. 7. Furthermore, fibers were pre-oxidized and annealed under Ar atmospheres to obtain Pt/MoC–CNF. The SEM and TEM images show that uniform size fibers are formed by electrospinning and HRTEM image show that dense nanoparticles with narrow size distribution can be seen across the entire CNF (Fig. 7 a-e). The AC HAADF STEM indicates that atomic size particles are anchored on the surface of MoC without any agglomeration (Fig. 7 f). The EDS mapping also confirms that Pt, C, Mo, N and O are uniformly distributed in the CNF (Fig. 7 g). The ICP-OES confirm the presence of 1.50 wt % Pt in CNF [44].

Using melamine-derived carbon nitride nanosheets (Pt-MCNs) and an electrospinning technique, Kim et al. reported a Pt SA catalyst system with 1D SnO₂ nano-heterostructure support, which shows excellent catalytic efficiency. Synthesis includes two steps i.e. formation of Pt-MCN through wet impregnation and reparation of Pt-MCN-SnO₂ nanofiber-in-tubes (FIT) by electrospinning and calcination. XAS, STEM, FT-EXAFS and XPS shows that the electrons transferred from Sn reduce the Pt species making them metallic. Pt SAs are not only highly stabilized by MCNs, but also trapped in the heterojunctions of the MCN/SnO₂ heterostructure. As a gas sensor, Pt-MCN-SnO₂ showed one of the world's best responses to formaldehyde gas. Moreover, it has an excellent stability which, even after >170 h of gas-sensing activity at 275 °C, shows only 7.1% degradation [45]. Wang et al. reported the synthesis of single

Pt atom supported on CeO₂ and showed high catalytic performance [46].

2.2. Synthesis of single Pd atoms on metal oxide supports

The noble metal catalysts like Pd and Pt (size 2–3 nm) are active for CO₂ reduction but they suffer from high scarcity and low atomic efficiency. To address these problems, great efforts have been made to prepare single atoms with the support. Recently, Geng et al. reported the synthesis of mesoporous TiO₂ supported Pd single atoms by a simple and large-scale spray assisted method. In details, HCl, F127, Pd(NO₃)₃ and tetrabutyl titanate were added into deionized water and mixed ultrasonically. The mixture was sprayed in a tube furnace and powder was collected by a filter paper collector and calcined at 400 °C in air. By increasing the concentration of Pd precursor, Pd NPs are formed instead of single atoms. The TiO₂ supports are mesoporous microspheres with anatase phase and possess large surface area. The mesoporous nature provides enough space for loading of single Pd atom up to 4.08 wt%. The HAADF-STEM shows that Pd single atoms are dispersed on TiO₂ matrix. AC HAADF-STEM image shows that single Pd atoms are loaded on TiO₂ matrix (Fig. 8b). The EDX mapping presents the uniform dispersion of Pd, O, Ti, and suggests the presence of atomically dispersed Pd atoms (Fig. 8a) [47].

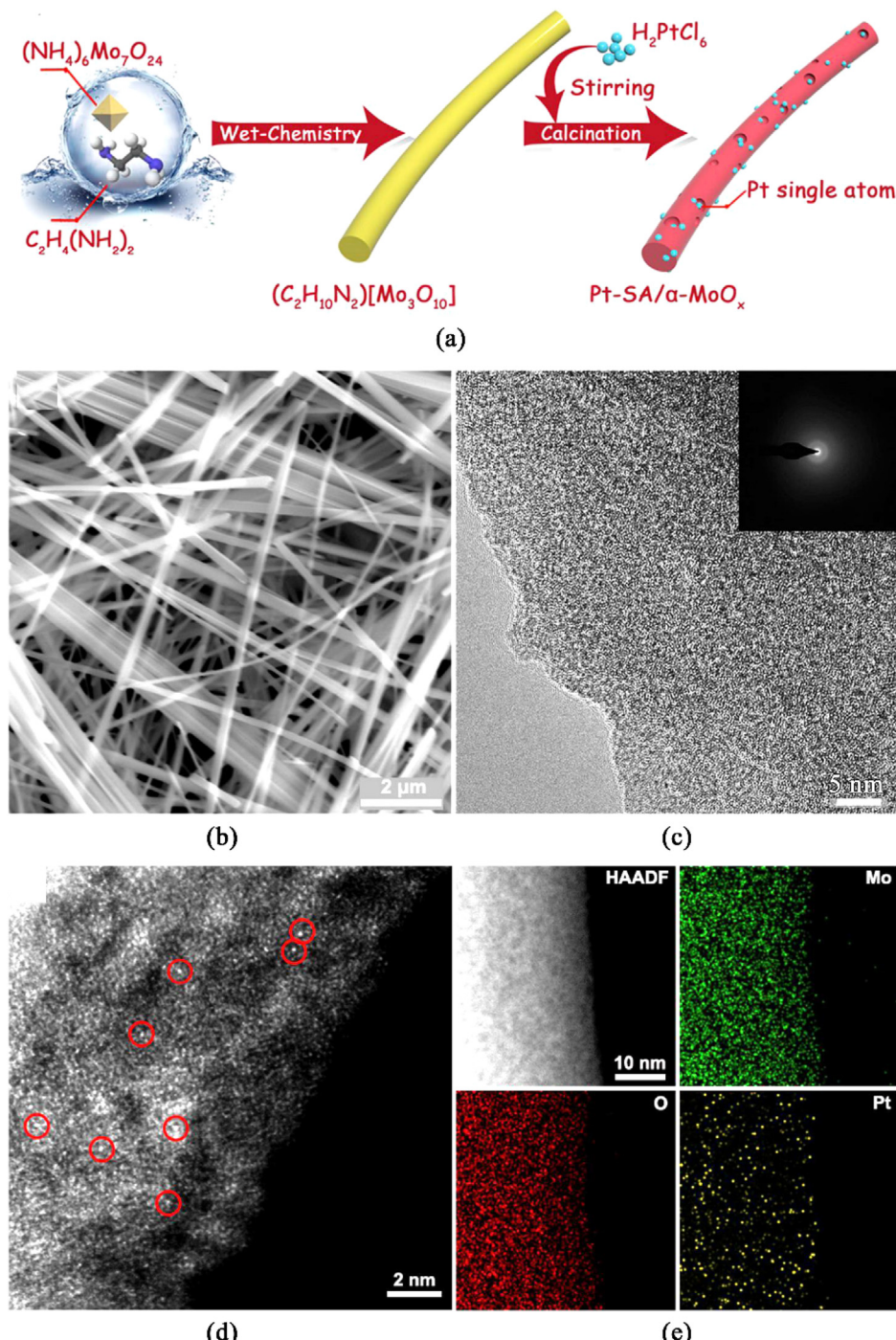


Fig. 6. Structures of Pt-SA/α-MoOx. (a) Schematic of the synthesis. (b) SEM image. (c) TEM image, in which is the corresponding SAED pattern. (d) Atomic-resolution HAADF-STEM image, in which some of the single Pt atoms are indicated by red circles. (e) EDX elemental mapping revealing the homogeneous distribution of Pt on Pt-SA/α-MoOx [43].

Guo et al. also reported the synthesis of single Pd atoms supported on TiO_2 prepared by photocatalytic reduction strategy. The homogenous mixture solution of TiO_2 and $\text{K}_2\text{PdCl}_4^{2-}$ was treated with liquid nitrogen to form an ice bulk. PdCl_4^- is deposited on the surface of TiO_2 nanoparticles through a heavy interaction between the electron-rich oxygen of TiO_2 and the empty orbitals of Pd metals. In order to excite TiO_2 , the ice bulk was irradiated with Xe light and created photogenerated electrons that facilitate the reduction of $\text{K}_2\text{PdCl}_4^{2-}$ to form Pd metallic species to a single atom assisted by TiO_2 for Pd. Pd NPs are formed instead of single atoms without freeze-drying and directly irradiation to Xe light. The STEM-EDS and HAADF-STEM results suggest that Pd metal is uniformly

distributed on TiO_2 substrate and present in the form of single atoms [48].

2.3. Synthesis of single Ir atoms on metal oxide supports

Zhang et al. reported the synthesis of single Ir atom on the FeOx support with a low loading of 0.01 wt % of Ir content by a coprecipitation method. H_2IrCl_6 and $\text{Fe}(\text{NO}_3)_3$ were used as the precursors of Ir and Fe, respectively. In details, under stirring at 80 °C the aqueous solutions of H_2IrCl_6 and $\text{Fe}(\text{NO}_3)_3$ with appropriate ratio were added into the NaOH solution and the pH of the solution was controlled around 8. After stirring

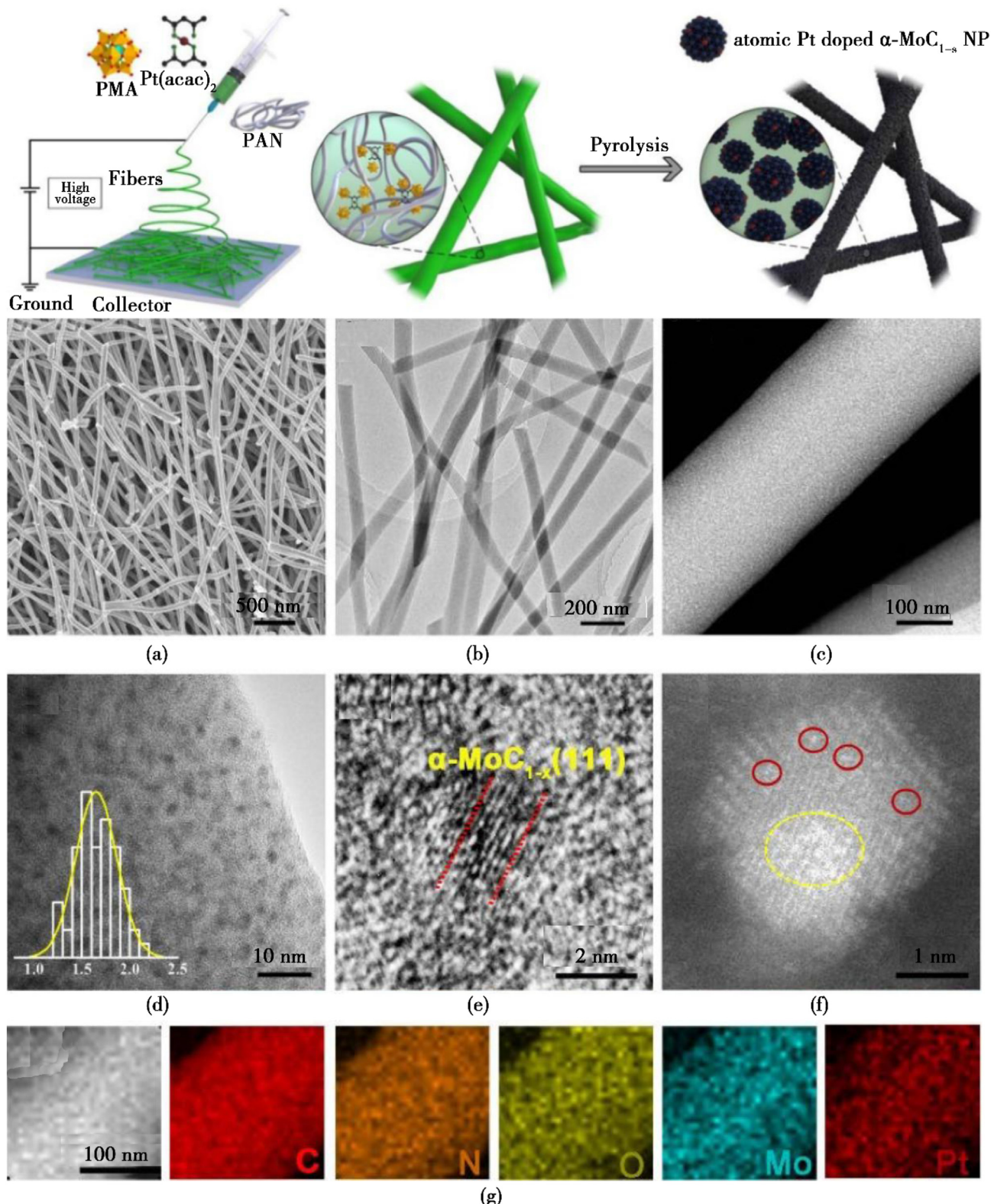


Fig. 7. Schematic illustration for the preparation of Pt/α-MoC_{1-x}-CNFs. (a) SEM, (b) TEM, (c) HAADF-STEM and (d) HR-TEM images of Pt/α-MoC_{1-x}-CNFs, the inset in d is the size distribution of α-MoC_{1-x} NPs in the CNF. (e) HR-TEM and (f) Aberration-corrected HAADF-STEM images of one single α-MoC_{1-x} NP in the CNFs, with single atoms of Pt marked in red circles and Pt clusters highlighted in yellow. (g) The corresponding element mapping of C, N, O, Mo, Pt in Pt/α-MoC_{1-x}-CNFs [44].

and aging for 4 h, the resultant precipitate was washed with water, dried overnight at 80 °C and calcined at high temperature of 300 °C in the presence of H₂/He mixture. The AC STEM was used to visually observe the single atoms and Ir single atoms can be identified with the FeOx

particles. The exact position of the iron atoms is retained by the single atoms of Ir. Due to low loading of Ir, it reduced the Ir-Ir interaction. Furthermore, a slight increase in the concentration of Ir up to 0.22 wt %, the Ir coexists in the form of single atoms and clusters. Furthermore, large

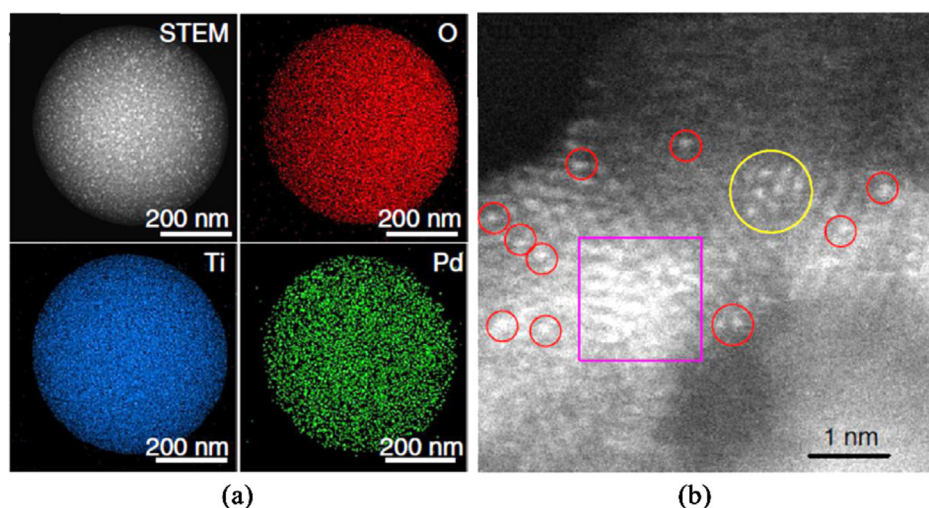


Fig. 8. HAADF-STEM-EDS mapping (a) and AC-HAADF-STEM image (b) of $\text{Pd}_{1+}\text{NP}/\text{TiO}_2$ [47].

particle clusters were observed by increasing the Ir concentration up to 0.35 wt % [49].

The stability and activity of the catalyst depend on interaction between catalyst and support. The support provides a platform where catalytic reaction occurs. Gu et al. reported the synthesis of high loading single Ir atom on a Nickel oxide (NiO) support. First they synthesized NiO on carbon cloth (CC), then treated with HNO_3 to remove impurities and washed with water to clean its surface. The cleaned CC was immersed in aqueous solution of $\text{Ni}(\text{NO}_3)_2$ and hexamethylenetetramine. The system was heated at 95 °C for 9 h, washed with water and dried. The dried CC was calcined at 350 °C for 2 h and cooled to room temperature. The NiO/CC was immersed into chloroiridic acid ethanol solution for 10 min and dried at 80 °C to grow Ir on NiO. The Ir–NiO/CC sample was obtained by calcination at 350 °C, cooling and washing with water several times. The prepared NiO was porous and ultrathin in nature (Fig. 9 a, b). The XRD pattern of NiO NSs did not change after high loading of single Ir atoms and it confirms that Ir did not dope into the bulk and remained mostly on the outermost surface (Fig. 9 c). The EDS and ICP-MS confirm that the loading percentage of Ir is almost 18 wt% (Fig. 9 f). The STEM image shows that Ir atoms are uniformly atomically distributed on the NiO NSs (Fig. 9 e, g) [50].

Li et al. also reported the synthesis of single Ir atoms on the TiO_2 oxide support. First, they synthesized TiO_2 NSs by hydrolyzing of TiCl_4 in ethylene glycol and these NSs are thermally reduced under hydrogen atmospheres to form polymorphs defective NSs with oxygen vacancies. The prepared NSs are metastable polymorphs of TiO_2 . The Ir single atoms on TiO_2 NSs were prepared by adding dropwise H_2IrCl_6 into well dispersed aqueous solution containing TiO_2 NSs (Fig. 10 a, b). The solution was stirred for 24 h and centrifuged. The obtained solid was washed with ethanol and water and reduced in H_2/N_2 mixed atmospheres. The ICP-OES analysis confirms that the percentage of Ir is 0.10 wt %. HAADF STEM and TEM images confirm that Ir cluster or particles are not present on the surface of NSs (Fig. 10 d). The AC HAADF-STEM shows that atomically disturbed isolated Ir atoms are present on the surface of NSs (Fig. 10 d). The homogeneous distribution of Ir was confirmed by the EDX analysis also (Fig. 10 c) [51].

2.4. Synthesis of single Au atoms on metal oxide supports

Single atoms supported on metal oxide support have much more sintering resistant, and higher reaction stability as compared to their NPs counterparts. Liu et al. reported the synthesis of single Au atoms supported on FeOx. In details, they synthesized FeOx support through a co-precipitation method. Under constant stirring at 50 °C, an aqueous solution of iron nitrate was added drop-wise in an aqueous solution of

sodium carbonate and the pH of the solution was kept around 8. The resulting precipitate was obtained by washing and filtration after stirring and aging for 3 h respectively. The obtained solid was dried at 60 °C and dispersed in water to prepare a support by a facile adsorption method. The HAuCl_4 solution was added dropwise under constant stirring in above solution. The sample was stirred for 2 h and further aged for 2 h. The gold supported on FeOx was obtained by washing, filtrating and drying at 60 °C. By increasing the concentration of Au, Au NPs on FeOx support were obtained. The AC HAADF confirm that gold atoms are uniformly dispersed on FeOx without the presence of Au clusters or NPs.

2.5. Synthesis of single Ru atoms on metal oxide supports

Single atoms exhibit superior catalytic performance and stability as compared to their nanoparticles. Various strategies have been developed to synthesize single atoms with metal support but bulk synthesis of single atoms is problematic. Zhang et al. reported the synthesis of thermally stable single Ru atoms from commercial RuO_2 powder and strong metal support. This simple and low cost method paves a way for thermally stable single atoms at large scale for industrial applications. The strong covalent metal support interaction promotes the transformation of RuO_2 powder to Ru single atoms. The spinel mixed oxide was used as a substrate. First, they prepared spinel oxide [$\text{MgAl}_{1.2}\text{Fe}_{0.8}\text{O}_4$ (MAFO)] by the solvothermal method and calcined at 700 °C to prepare as a support for the growth of single atoms. The single atoms of Ru supported on MAFO were prepared by heating the ruthenium (III) acetylacetone with MAFO support at 900 °C. The AC HAADF-STEM confirmed the uniform dispersion of single Ru atoms on MAFO support. The lower temperature calcination of ruthenium (III) acetylacetone with MAFO support at 500 °C results in the formation of RuO_2 aggregates [52]. Song et al. reported the synthesis of Ru single atoms supported on the Ni_5P_4 . In details, they prepared Ni(OH)_2 with rich nickel vacancies by a propylene oxide-mediated alkalization precipitation method. The Ru^{3+} cations were stabilized on the surface by wet impregnation methods as shown in the schematic diagram (Fig. 11 a). The abundant Ni vacancies in Ni(OH)_2 played a vital role for the impregnation of single Ru atoms. The ratio of Ru single atoms is less on Ni(OH)_2 with less Ni vacancies on Ni(OH)_2 while the high loading of Ru single atoms stabilized on the high vacancies of Ni on Ni(OH)_2 . The XRD pattern confirms that Ru related species peaks were not present and Ru species are highly dispersed on the surface and peak patterns well matched with Ni_5P_4 . The HRTEM showed two continuous lattice fringes corresponding to (201) and (004) planes of Ni_5P_4 (Fig. 11 b). The HAADF STEM image shows the atomically dispersed bright spot that confirms the presence of Ru single atoms and the uniform distribution of Ni, P and Ru was also revealed by elemental

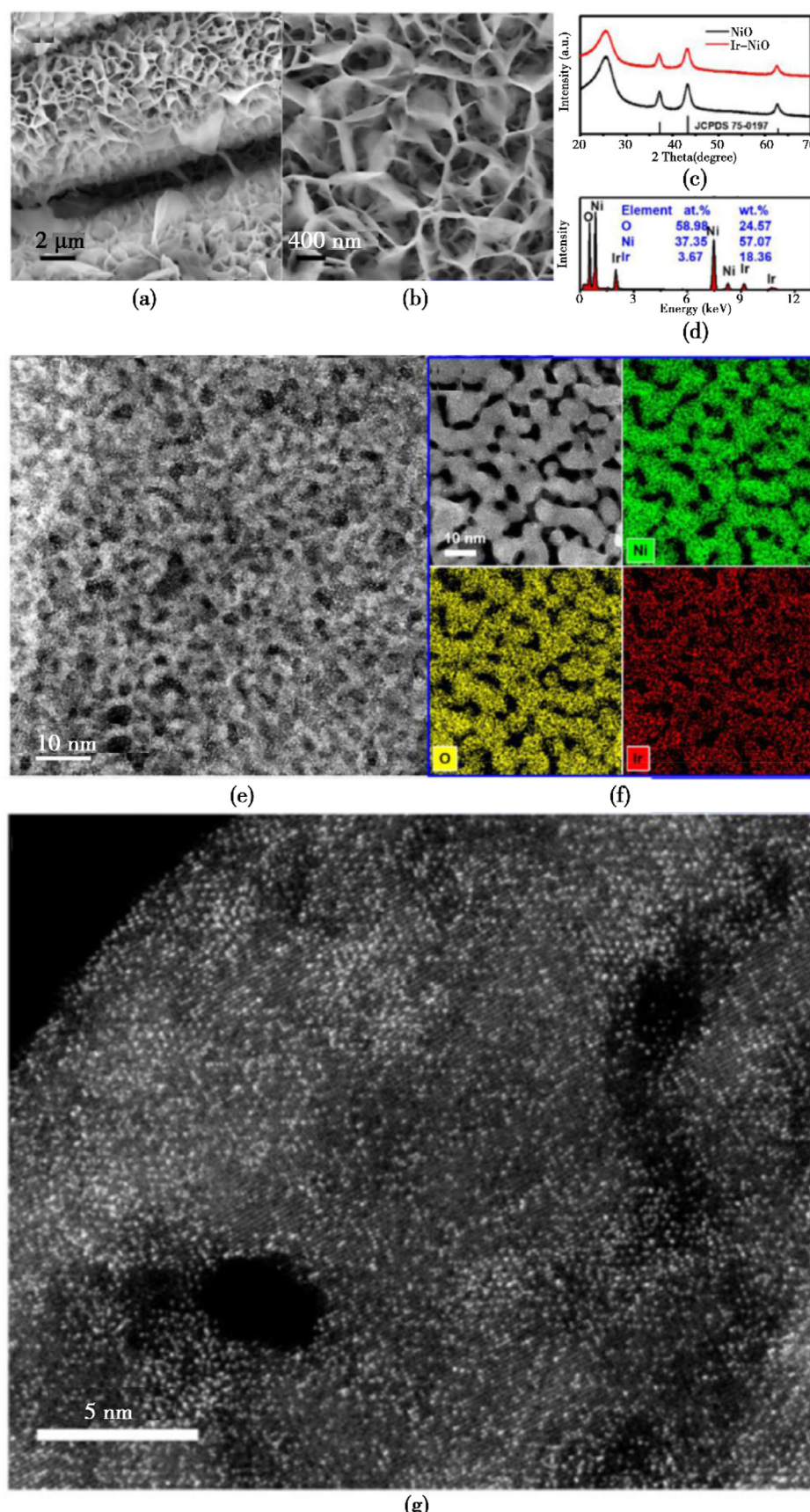


Fig. 9. (a, b) Representative low (a) and high (b) magnification SEM images of Ir–NiO sample. (c) XRD patterns of NiO and Ir–NiO. (d) EDS spectrum of Ir–NiO. (e) Representative low and (g) high magnification HAADF-STEM images indicating high density of Ir single atoms. (f) STEM-EDS elemental mapping of Ir–NiO [50].

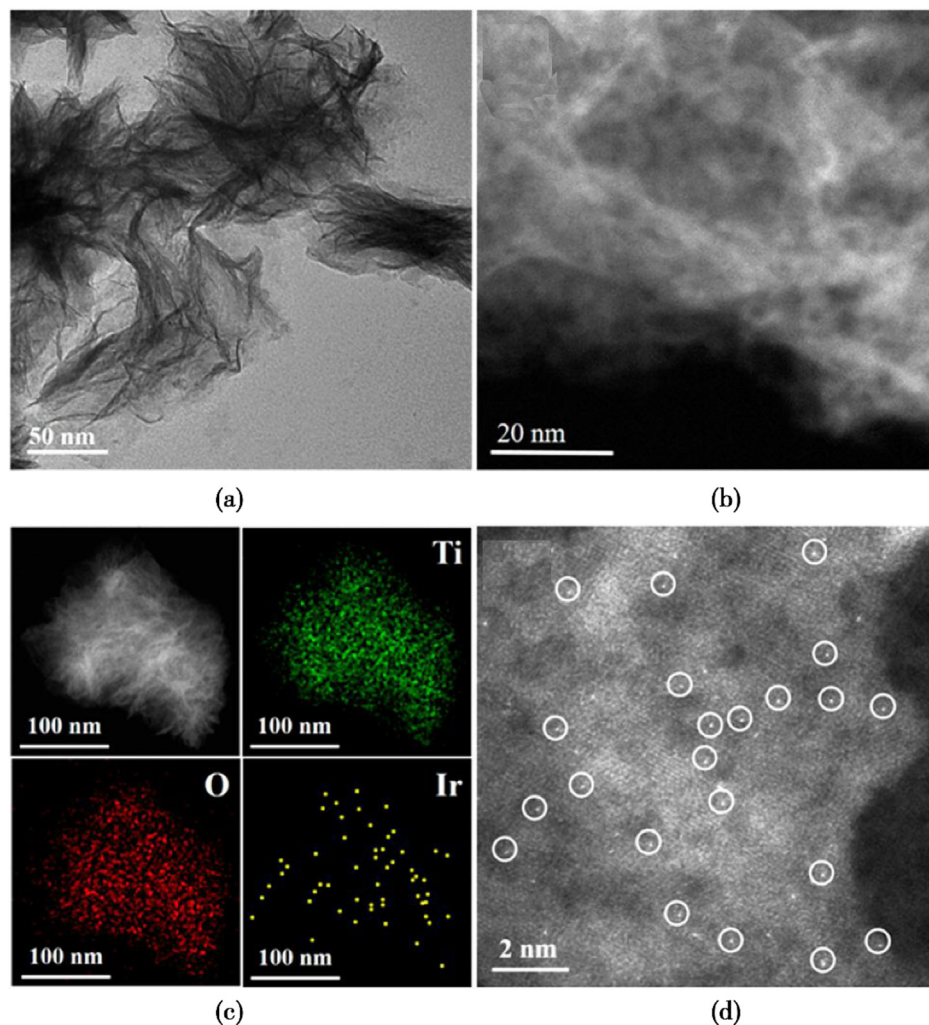


Fig. 10. Characterization of $\text{Ir}_1/\text{def}-\text{TiO}_2$. (a) TEM image of the $\text{Ir}_1/\text{def}-\text{TiO}_2$ nanosheets. (b) HAADF STEM image of $\text{Ir}_1/\text{def}-\text{TiO}_2$ nanosheet. (c) EDX elemental mapping analysis for the distributions of Ti (blue), O (red), and Ir (green), respectively. (d) AC HAADF-STEM image of the $\text{Ir}_1/\text{def}-\text{TiO}_2$ sample [51].

mapping (Fig. 11 c, d) [53].

2.6. Synthesis of single Co atoms on metal carbide supports

Due to the co-ordination environment of active atoms and high utilization performance, single atoms with sufficient support are one of the most active frontiers in catalysis. Recently, Wang et al. reported the sacrificial Zn strategy to grow single atoms on the support. Zn/Mo bimetallic imidazolate (BIFs) has been transformed by thermal annealing to holey 2D MoC and Zn is vaporized to generate the desired porous structure with a high exposed surface area. The metal vacancies are formed on the surface of MoC by Zn atoms vaporization and these vacancies facilitate the migration and anchoring of single metal atoms on the MoC surface. The Zn atoms were first partially substituted from Mo/Zn BIFs and single atoms of transition metals were anchored on MoC surface by pyrolyzation as shown in the schematic diagram (Fig. 12 a, b). The MoC has 2D holey morphology as confirmed by FESEM and STEM (Fig. 12 c-e). The HAADF STEM shows the isolated dark dots on the surface of MoC that confirm the existence of Co single atoms (Fig. 12 h). The loading amount of Co is 1.78 wt% as verified by ICP [54].

2.7. Synthesis of single Ni atoms on metal oxide supports

Several synthesis methods have been utilized to synthesis single atoms catalysts. Wang et al. recently reported the synthesis of single atom

Ni distributed on TiO_2 support by a molten salt method (Fig. 13 a). The metal salt (a mixture of LiCl and KCl) makes an atomic dispersion of Ni^{2+} ions by heating metal salt at its melting point on TiO_2 surface and the polarizing force provided by molten salts eases the destabilization of Ti–O bonds and facilitate the formation of Ni–O bonds on the surface of TiO_2 . Furthermore, this low-temperature heating prevents the damage of TiO_2 nanostructure and aggregation of Ni atoms. The molten salt method also facilitates the formation of oxygen vacancies that are beneficial for catalytic reactions. By heating the precursor of $\text{Ni}(\text{NiCl}_2 \cdot 6\text{H}_2\text{O})$, TiO_2 nanoparticles and a mixture of salts (LiCl and KCl) in a semi-capped corundum crucible at 773 K for 2 h under N_2 flow, the Ni single atoms assisted by TiO_2 support synthesis. The mixture of salt (LiCl and KCl) makes liquid phase by heating at fusion point where NiCl_2 dissolves and disperses atomically in this solution. The molten salt also forms high dispersion of TiO_2 nanoparticles due to space confinement effect. The surface oxygen of TiO_2 nanoparticles becomes metastable due to polarizing force provided by molten salts and the surface oxygen of TiO_2 nanoparticles making Ni–O bonds with free moving Ni^{2+} ions. After cooling naturally, washing with water and removing salt the desire products of Ni single atoms supported on the TiO_2 were obtained as shown in the schematic diagram (Fig. 13 a). The AC-STEM reveals the presence of atomically dispersed Ni on the surface of TiO_2 (Fig. 13 b-e). The EDS analysis also confirms the presence of Ni single atoms on the surface of TiO_2 [55].

Single atoms with metal support exhibit superior catalytic activity,

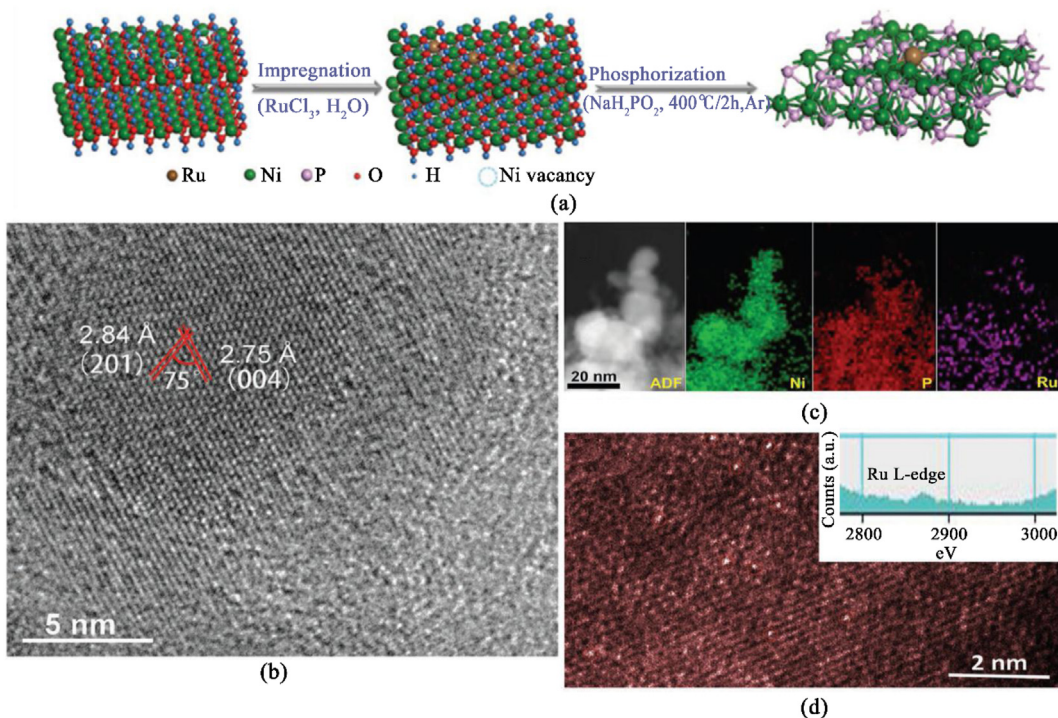


Fig. 11. a) Schematic diagram for the synthesis of Ni₅P₄-Ru. b) HRTEM image of Ni₅P₄-Ru. c) Elemental mappings of Ni₅P₄-Ru. d) HAADF-STEM image of Ni₅P₄-Ru (inset: corresponding EELS spectrum at Ru L-edge) [53].

catalyst stability and advanced microscopic characterization like ACTEM are mostly used to study their role in catalysis. However, only microscopic characterizations are unable to provide the atomistic view of the bonds that attach with the surface and their catalytic role. But, by combining various characterization with Density functional theory (DFT) calculations, precise information about catalysis could be obtained. Zheng et al. had predicted the catalyst structure at atomic level for electrochemical CO₂ reduction of Cu single atoms supported on the CeO₂ with enriched oxygen vacancies (Fig. 14). They used the first principle method to calculate adsorption energy of CO₂ on the surface of Cu single atoms supported on the CeO₂. Oxygen vacancies are formed spontaneously to maintain the charge balance as Cu⁺² replaced Ce⁺⁴-O⁻² on the (110) surface. Interestingly, the formation energy of oxygen vacancy is also favorable for the formation of second and third oxygen vacancy. By increasing further oxygen vacancies, structure destabilized. The DFT calculations reveal that Cu sites associated with 2 or 3 oxygen vacancies are liable for CO₂ adsorption. The Cu sites with 3 oxygen vacancies are the most favorable sites for CO₂ adsorption due to bend structure while undoped CeO₂ and Cu with one or two oxygen vacancies present original molecular structure and have high adsorption energy for CO₂ reduction (Fig. 14) [56].

3. Application in CO₂ reductions

The reckless production of CO₂ is being a global challenge for the environment and poses serious threats to life. The U.S. National Oceanic and Atmospheric Administration (NOAA) and Scripps Institution of Oceanography reported that environmental CO₂ production peaked at 417.1 ppm and 417.2 ppm respectively. The average production rate was 0.8 ppm in the 1960s and 2.0 ppm in the 2000s, rising to 2.4 ppm in the last decade, with an overall increase in environmental CO₂ of around 149% compared to the pre-industrial era (Fig. 16) [58]. The increased amount of CO₂ causes a greenhouse effect, which increases the temperature of the planet by absorbing infrared radiation. To deal with the increasing CO₂, a variety of methods have been developed to reduce CO₂ and maintain a balance with environment. Among these methods, CO₂

reduction reaction (CO₂RR) gained a considerable attention because of its simplicity and the fact that it can produce valuable industrial chemicals and fuels. Plants are naturally doing this job via photosynthesis but there is a limit for their consumption. Traditionally Fischer-Tropsch syntheses is used to reduce CO₂ in the presence of H₂ gas, but H₂ production is commercially carried out via methane reforming, leaving the problem unaddressed. Catalytic processes e.g., photocatalysis and biocatalysis are also being investigated but the low yields and high cost hampers their practical applications.

CO₂RR has potential to become future technology to get valuable products that may meet the industry demand and eradicate the use the conventional fossil fuel sources. Some of the common CO₂RR products include methane (CH₄), monoxide (CO), methanol (CH₃OH), formic acid (HCOOH), ethanol (C₂H₅OH) ethylene (C₂H₄). Fig. 17 (a) shows the current industrial production approaches of these products along with electrochemical CO₂ reduction with respect to number of electrons required to get these products. For their industrial production, in most cases high pressure or high temperature is required, that makes the process costly. Electrochemical reduction may cut the production cost due to benign conditions and avoiding the use of fossil fuels as raw materials [59]. CO₂ because of its high C=O energy (806 kJ/mol) makes it very stable under normal conditions and requires harsh conditions for reduction. Several intermediates are involved in CO₂RR and may have multiple electron and proton transfer steps. Several metals have been explored for CO₂RR for methanol, ethanol, methane, formic acid, and carbon monoxide production. A chart (Fig. 17 b) is shown below for metal electrocatalysis and their corresponding products with color coding. Some metals give more than one product e.g. Sn may produce formic acid and carbon monoxide and Cu produces methane, methanol and ethanol. Cu, Ag and Au have been explored for C1+ products [60,61].

Types of products and mechanism of CO₂RR depend on multiple factors including nature of catalyst, pH of system, electrolysis conditions, nature of adsorption interaction etc. G. Xing and co-workers investigated spin-polarized DFT method to study SACs based CO₂ reduction for M₃ (hexahydroxybenzene)₂ Where M = Cr, Ru, Rh and Mo etc. Exchange-correlation energy was calculated by Perdew-Burke-Ernzerhof (PBE)

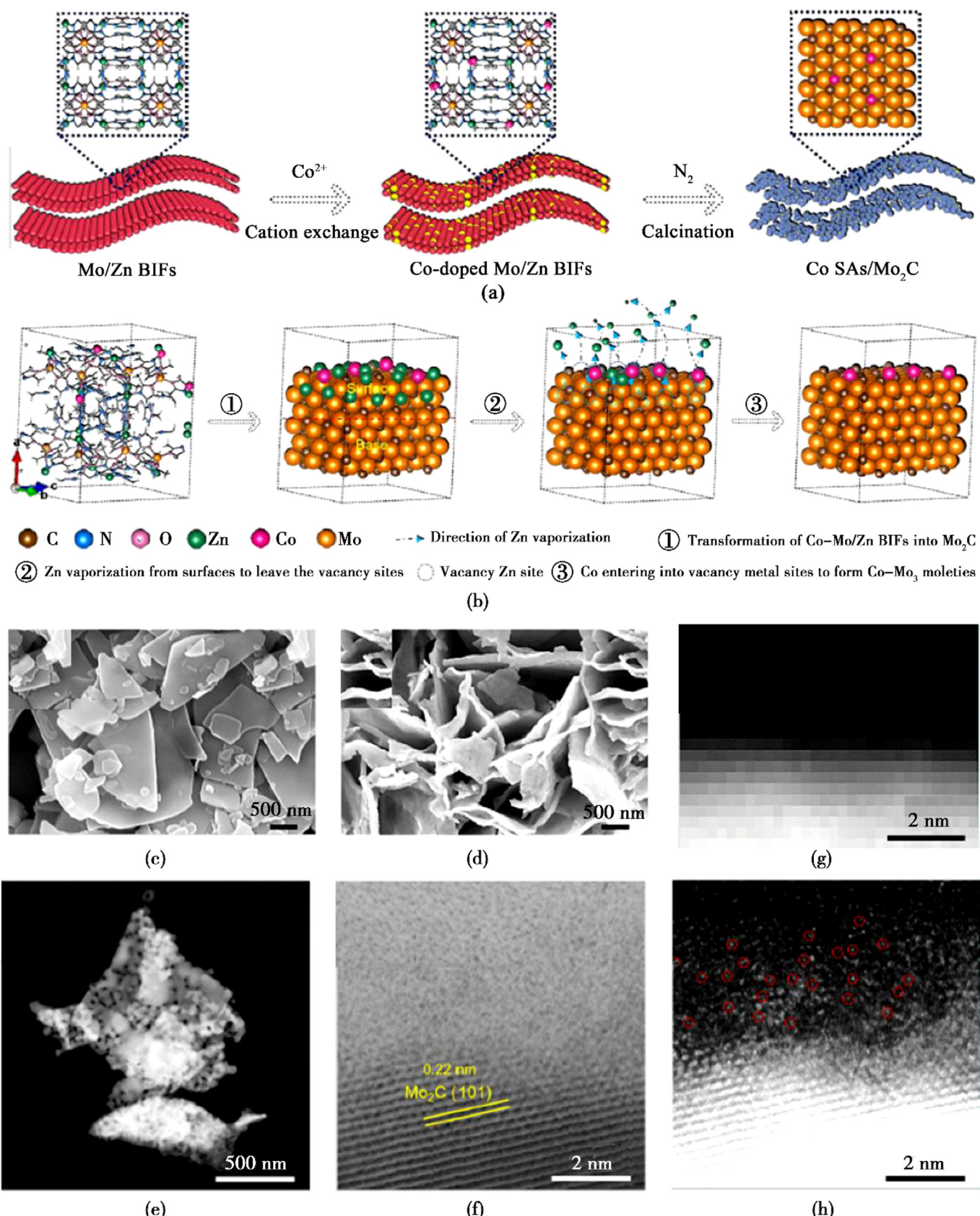


Fig. 12. (a) The schematic illustration of the synthesis of Co SAs/Mo₂C. The enlarged details on atomic configurations are inserted. (b) Schematic formation mechanism of Co-Mo₃ moieties on the surface of Mo₂C. (c, d) SEM images of Co-Mo/Zn BIFs. (e) STEM image of Co SAs/Mo₂C. (f, h) High-resolution bright-field (f) and dark-field (h) STEM image at EELS-mode of Co SAs/Mo₂C. g) HAADF-STEM image at EELS-mode of Co SAs/Mo₂C [54].

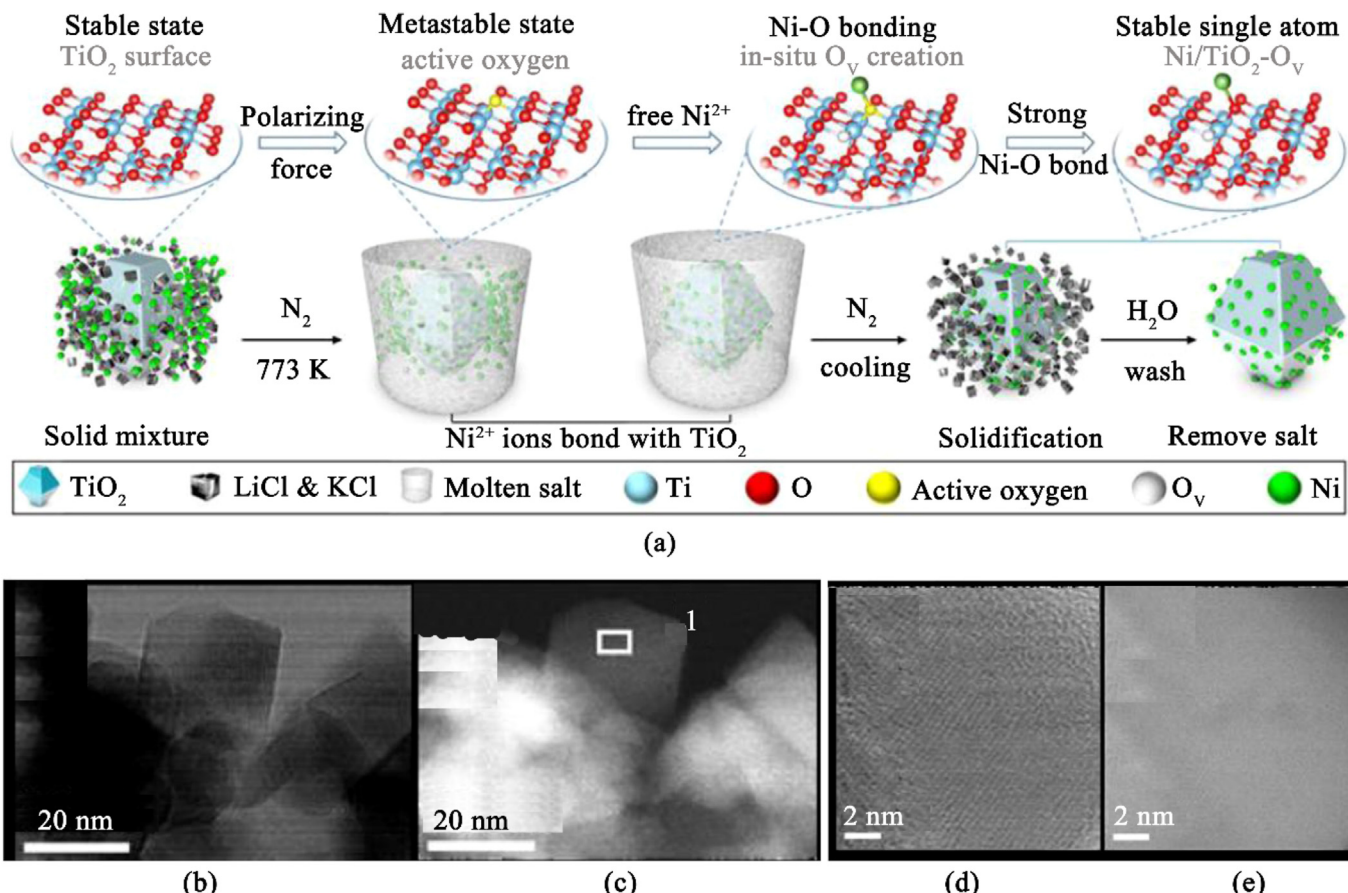


Fig. 13. (a) Schematic illustration of molten salt mediated preparation of atomic Ni on TiO₂. For the TiO₂ molecular structure, blue balls and red balls represent Ti and O atoms, respectively. AC-STEM bright-field (b, d) and dark-field (c, e) images [55].

functional form by generalized gradient approximation. Gibbs free energy change (ΔG) was calculated by the computational hydrogen electrode model. Cu because of its limiting overpotential of -0.61 eV is considered as best candidate for CO₂ to CH₄ reduction; thus, it was taken as reference. In the system M₃(H₂COO)₂ (where M = Mn, Fe, Co, Ni, Cu, Pd, Ag, Re, Os, Ir, and Pt) shows high ΔG and hence conclude they interact weakly with *HCOO and *COOH intermediates. The role of these intermediates is crucial, as they fall at the first step of interconversion or reduction. So, these metals were excluded due to their weak catalytic activity. Mo, Ru, Rh, Cr and W have comparatively low energy barriers exhibiting better capability of catalysis. Their study suggests that *HCOO is relatively more stable in comparison with *COOH for Cr, Mo and W, whereas *COOH is only favored in case of Rh and Ru [62]. Yang and co-workers summarized these reaction pathways for different products based on recent studies. CO₂RR occurs at low overpotentials for CO or HCOOH products as they are two-electron transfer products and the easiest to target. For HCOOH formation by proton-coupled electron-n-transfer (PCET) reaction *OCOH is the intermediate while for CO it would be *COOH. This reaction pathway strongly influence the final products e.g., in case of Au and Ag, CO is obtained while Bi and In produce HCOO⁻. However, for multi-electron products this process become sluggish and control over selectivity is decreased. Reaction pathways for common C1 and C2 products are shown in the Fig. 18 [15].

In 1985 Shin et al. reported the first electrochemical reduction of CO₂ into CO and CH₄ in aqueous hydrogen carbonate solution. Several metals have been explored for CO₂RR and are grouped based on the types of products e.g. Fe, Ni, Pt, Al involves in hydrogen evolution whereas Zn, Ag and Ag produce CO and Cu gives various hydrocarbons. To improve the energy efficiency and selectivity towards products, materials size, shape and morphologies are finely tuned and manipulated on nanoscales.

Nanostructuring of materials boosts the catalytic activity due to high surface to volume ratio, actives sites and edges. Moving a step ahead to the new regime of heterogeneous catalysis, researchers are making efforts to stabilize single-atom catalysts (SACs). Single atom catalysts can be prepared via a) immobilizing metal ions on oxides b) trapping the metal atoms in MOFs, COFs or other porous materials. These single metal site catalysts offer selectivity towards one carbon products e.g. CO and HCOO⁻ [14].

The metal support interaction (MSI) has great influence on the catalytic properties. The MSI gives insight of activation and stabilization of dispersed single metal atoms. Due to metal oxide support, the isolated metal atoms would be vulnerable to aggregation during preparation and the catalytic process. Based on the combination of experimental observation and DFT calculations, the bonding between the metal oxide support and the metal is stronger than that of the metal itself, and due to this metal atoms tend to be finely dispersed instead of aggregated. On suitable oxide supports, isolated metal atoms have been more firmly anchored on the oxides than their cluster/NP counterparts [32]. Bao et al. reported CO₂ reduction using solid oxide electrolysis cell with cathode made up of Pd single site anchored La_{0.5}Sr_{0.5}Fe_{0.8}Sm_{0.202-x} (LSF-samarium doped ceria (SDC)). The CO₂ reduction is enhanced by 65.7% by doping Pd single atoms to LSF as compared to only LSF-SDC cathode. The CO₂ electrocatalysis was carried out in solid oxide electrolysis cells (SOECs). With the increase in applied voltage-current densities increase gradually (Fig. 19). Introduction of Pd in nanocomposite improves catalytic activity and 0.8% Pd-LSF(SDC) gives the best results as compared to other Pd concentration variables in the composite. At 1.6 V, the highest current density is 0.58 acm², which is 65.7% higher than the LSF (SDC). CO production rate surges with the increase in applied voltage and it increase the CO production at 1.6 V from 2.60 to 4.0 mL min⁻¹ cm⁻²,

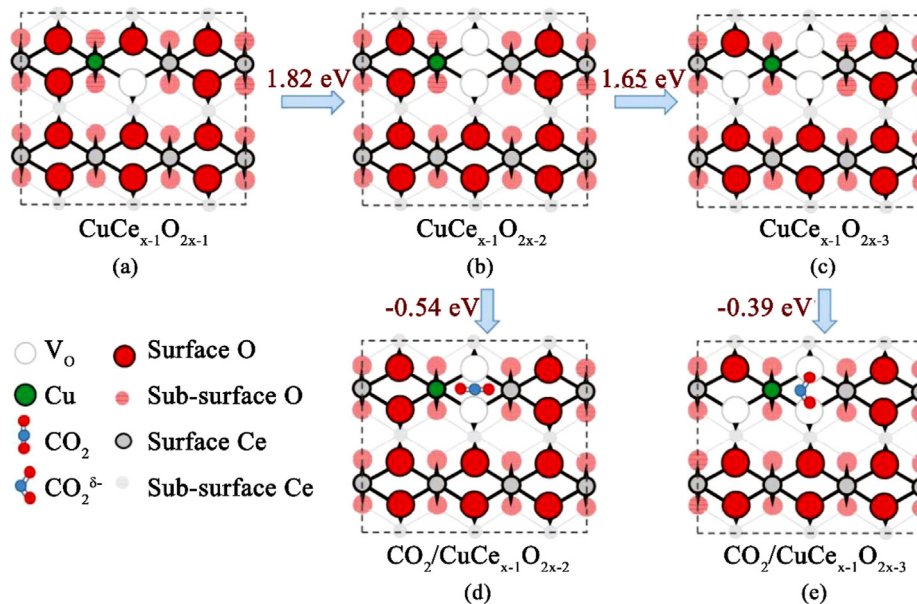


Fig. 14. Theoretical calculations of the most stable structures of Cu-doped $\text{CeO}_2(110)$ and their effects on CO_2 activation. (a–c) Structure models of $\text{CeO}_2(110)$ doped with one single Cu site, with (a) 1 oxygen vacancy (V_o); (b) 2 V_o 's; and (c) 3 V_o 's. (d, e) Structure models of these V_o -bound, single-atomic Cu site on CeO_2 for CO_2 adsorption and activation. The energy differences associated with each structure change were also specified. The formation energy for 1 V_o on a pure $\text{CeO}_2(110)$ was calculated to be 1.74 eV, indicating that the 3 V_o -bound structure (c) is the most stable for the single-atomic Cu site on CeO_2 [56]. Recently, Bao et al. had synthesized Pd single atoms supported on perovskite and the material shows remarkable activity for CO_2 electrocatalysis. They used DFT calculations to measure the potential energy landscape of CO_2 electrolysis on Fe and Pd centers, and the corresponding intermediates are shown in Fig. 15. They compared the adsorption energy of CO_2 for all three systems including Fe with coordination number (CN) 4, single atom Pd supported on perovskite with CN 2 and CN 3. The Pd single atoms supported on perovskite with CN 2 played a crucial role in CO_2 reduction and the site has lowest adsorption energy because coordinatively unsaturated Pd atoms together with oxygen vacancies made an active center to adsorb and activate CO_2 . Further, the nature of active center and dissociation process were studied by electronic structure. The CO_2 is adsorbed on Pd single atoms with CN 2 through C–Pd bond (see red area), a mild O1–Pd bond and O_2 vacancy coalition as depicted by electronic difference map. The dissociation group of CO species is attached with Pd while O_2 are filled with vacancy to complete the dissociation process. Furthermore, the d-orbital projected density of state (DOS) study shows that Pd single atoms with CN 2 DOS is more abundant around the Fermi level as compared to other two. The DFT study confirmed that single atoms Pd with CN 2 is the most favorable site for CO_2 adsorption and activation (Fig. 15) [57].

when the Pd concentration reaches 0.8%. DFT calculations and electrochemical studies support the argument that the activity is due to single-site anchored Pd atoms and the metal atoms tend to be finely dispersed instead of aggregation [14].

Gu et al. reported the electrochemical conversion of CO_2 to CO using iron SACs. The Fe catalyst (Fe^{3+} —N—C) was synthesized by pyrolyzing Fe-doped zinc (Zn) 2-methylimidazolate framework (ZIF-8) at 900 °C under nitrogen flow. Inductively coupled plasma optical emission spectrometry (ICP-OES) revealed the weight fractions of Zn and Fe 3.4% and 2.8%, respectively. Linear sweep voltammetry (LSV) curve of Fe catalyst shows that the onsite potential is more positive than −0.20 V versus reversible hydrogen electrode (RHE) in a KHCO_3 0.5 M saturated electrolyte. A control sample of Zn prepared from pyrolysis of ZIF-8 under same conditions except the presence of Fe shows almost negligible current density makes it clear that the catalytic activity is due to the presence of Fe. The electrocatalytic activity in H-cells was tested, the only products obtained were CO and H_2 . The use of gas diffusion electrode (GDE) increased the j_{CO} to 94 mA cm^{-2} compared to 20 mA cm^{-2} in H-cell, this could be due to better mass transport. The Faradic efficiency for CO on cathode also improved to 90% (as compared to 80% in H-Cell). The catalyst was stable between −0.2 and −0.5 V with reproducible results under variations e.g. when electrolyte purity was changed and used tap water [63].

Hengpan Yang et al. reported the conversion of CO_2 into methanol using carbon membranes embraced with copper SACs. Polyacrylonitrile

(PAN, $M_w = 130,000$) and Cu/ZIF-8 solution were electrospun and carbonized to get Cu SAs through carbon nanofibers CuSAs/TCNFs and CuSAs/CNFs. FE-SEM and TEM images show the diameter of TCNFs is about 700 nm with uniform internal hollow nanoholes with a diameter of 100 nm. HAADF-STEM shows that the Cu and N atoms are uniformly distributed over the CNFs and the amount of Cu on CNFs and TCNFs measured by inductively coupled plasma optical emission spectroscopy (ICP-OES) were 1.4 and 1.3 wt% respectively. X-ray photoelectron spectroscopy (XPS) studies revealed that the oxidation of Cu species is between 0 and +2. The uniform distribution, high stability and high percentage of Cu single atoms on TCNFs make the catalyst superior and offer excellent catalytic activity. The electrochemical studies for CO_2RR were carried out in a two-compartment electrochemical cell with Nafion as proton exchange membrane (PEM). Cu SAs/CNFs have very low activity as compared to CuSAs/TCNFs despite having similar wt% of Cu atoms. This clearly indicates that the activity is boosted by the nanoholes present in CuSAs/TCNFs catalyst. It is manifested by CO_2 adsorption capacity and electrochemical active surface areas (ECSA) comparison of two catalysts. The ECSA of CuSA/CNFs is 7.2 mF cm^{-2} while for CuSAs/TCNFs is approximately three times greater i.e. 23.3 mF cm^{-2} . Also, CO_2 adsorption capacity for CuSA/CNFs is 20 times lower than that of CuSAs/TCNFs. Consequently, it is obvious from these evidences that the nanoholes play crucial role for the superior activity of CuSAs/TCNFs by providing CO_2 free way through these nanoholes towards CuSAs and by exposing them to catalytic activity. The Faradaic efficiencies (FEs) of

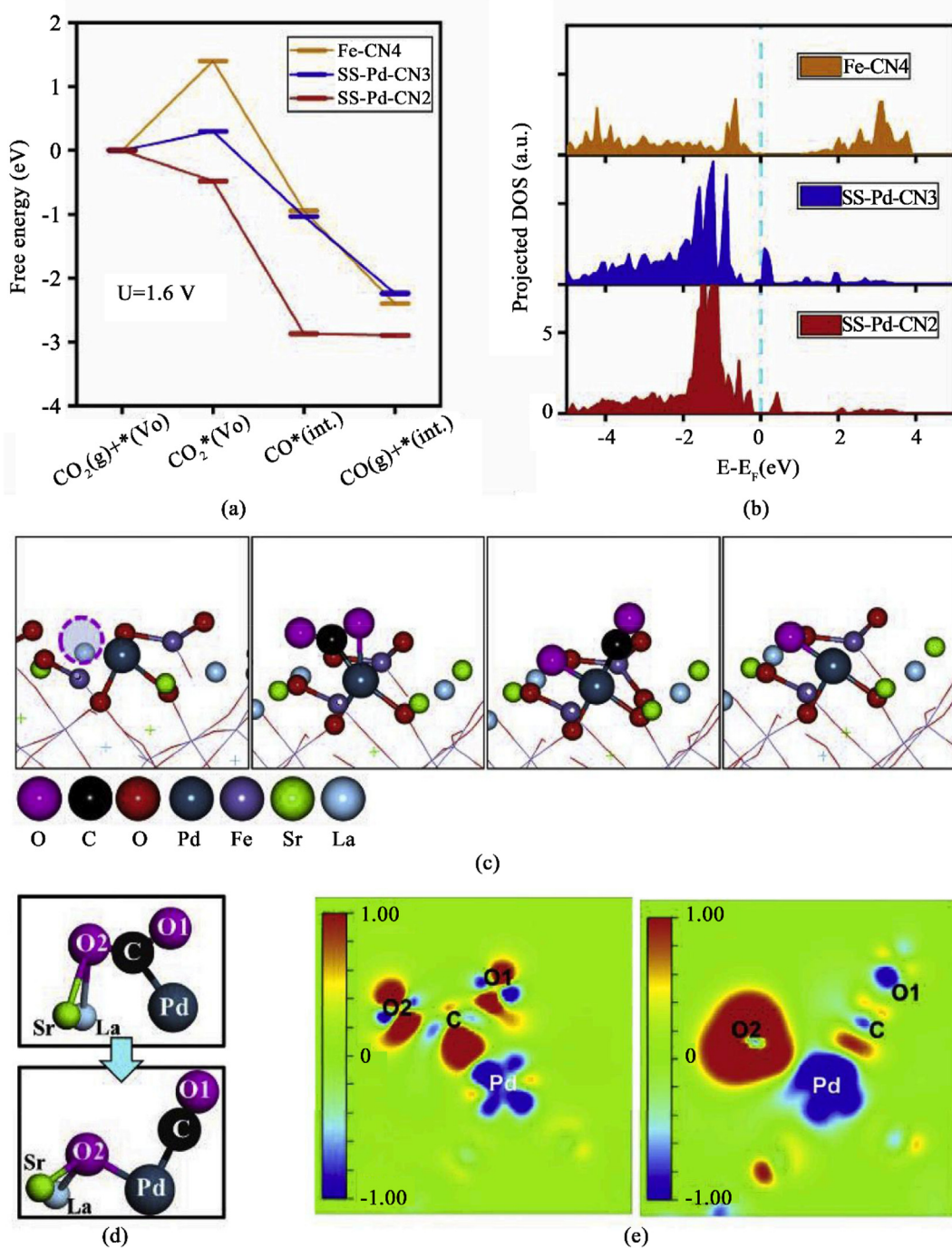


Fig. 15. Theoretical analysis of the CO_2 electroreduction to CO by DFT calculations. **(a)** Potential energy landscape of the CO_2 electrolysis process over the three sites: Fe-CN4 in LSF(110), SS-Pd-CN3 and SS-Pd-CN2 in Pd-LSF(110) at 800 °C and 1.6 V * (int.) and *(Vo) denote the site without and with one oxygen vacancy. **(b)** The sum of up and down-spin d-orbital projected DOS of active Fe and Pd atoms for the corresponding adsorption sites. The dashed cyan line marks the Fermi level. **(c)** Optimized atomic configurations of the CO_2 electroreduction to CO process over SS-Pd-CN2 (side view), which corresponds to the red line in **(a)**. The dashed pink circle denotes the oxygen 18 vacancy. **(d)** Amplified local atomic geometry truncated by $\text{CO}_2^*(\text{Vo})$ and $\text{CO}^*(\text{int.})$ of **(c)**. **(e)** 2D contour plots of the charge density differences for $\text{CO}_2^*(\text{Vo})$ and $\text{CO}^*(\text{int.})$ over SS-Pd-CN2. Red and blue regions denote increased and decreased electron densities, respectively [57].

CuSAs/TCNFs for methanol reached a maximum (44%) and for CO (56%) at $-0.9 \text{ V}_{\text{RHE}}$. Moreover, the catalyst maintained its electrochemical activity with negligible fall in current density without disturbing the morphology of catalyst when tested for 50 h [64].

An efficient and cost-effective Ni-based SACs supported on carbon nanoparticles for CO_2 to CO is developed by Tingting Zheng and co-workers. Ni^{2+} solution was added drop by drop into the commercial carbon black (CB) while stirring vigorously. The defects on the carbon

black nanoparticles and the presence of oxygen moieties helped to adsorb Ni^{2+} atoms. In Ni^{2+} -CB mixture, urea was added as a source of nitrogen and then heated at 800 °C to obtain Ni-NCB. The electrochemical reduction of CO_2 was carried out by three-electrode H-cell at potentials between -0.3 and -1 V vs RHE. The FE obtained for CO was 95% at -0.6 to -0.84 V vs RHE and selectivity was 99% at -0.68 V vs RHE whereas the control experiment with the similar catalyst without Ni atoms shows negligible activity. As mass transport in H-cells is limited and large over-

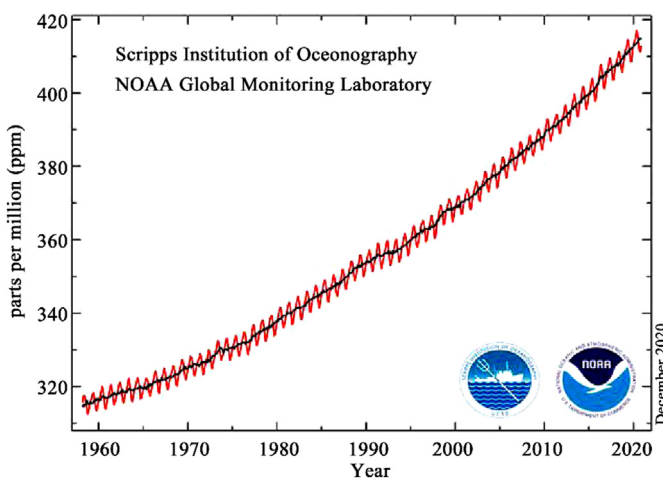
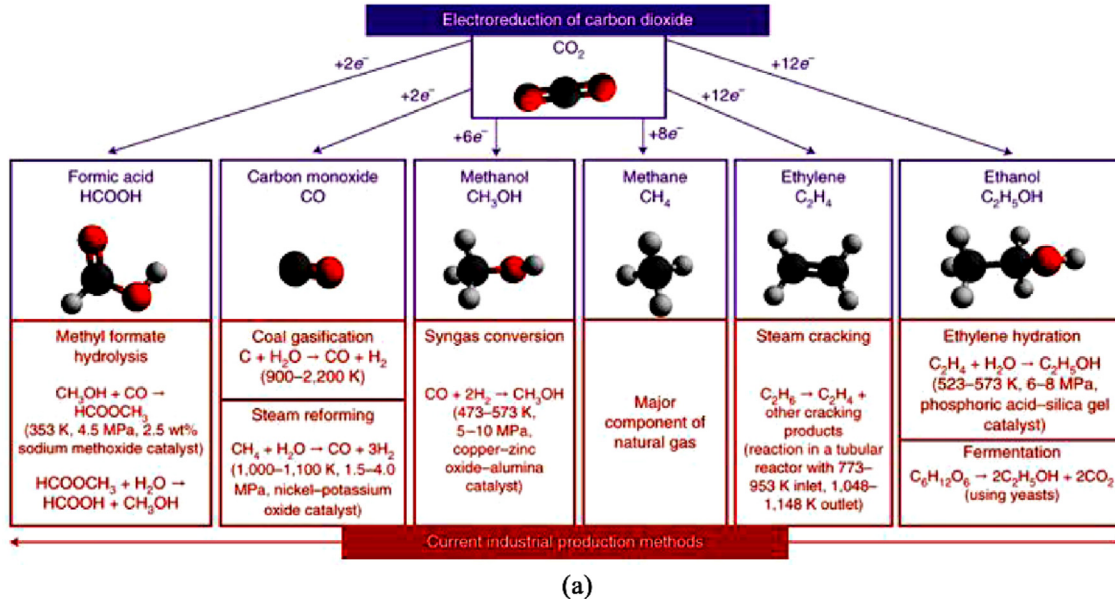


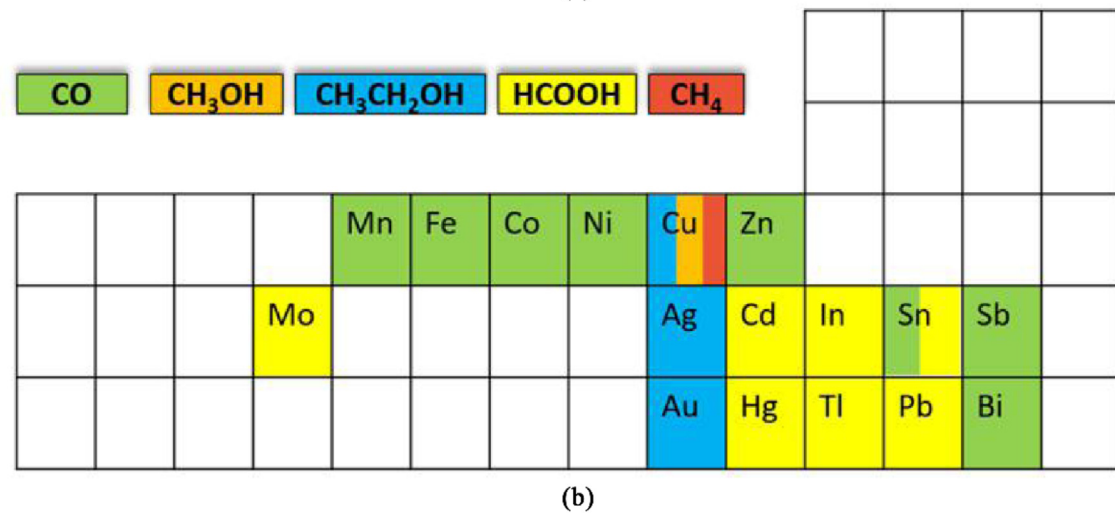
Fig. 16. CO₂ measure from March 1958 to December 2020 at Mauna Loa Observatory, Hawaii. Red lines represent monthly trends whereas black lines present averaged values [58].

potentials are observed due to higher kinetic current. The fuel cell strategy was also applied to test the catalytic activity and the catalyst was observed to have an efficiency of almost 100% and a current density of up to 130 mA cm⁻². So, the CO₂RR activity is attributed to the single-atoms supported on the CB. It was also verified by tuning the conditions, e.g. changing the nitrogen source to NH₃ decreases the activity and changing the Ni²⁺ concentration leads to the growth of nanoclusters and hence reduces the activity [65]. Zhong and coworkers demonstrated another protocol to stabilize Ni single-atoms utilizing covalent-organic frameworks (COFs) for CO₂ to CO reduction under visible light. They synthesized Ni loaded 2, 2'-bipyridine-based COF (Ni-TpBpy) and obtained good yields i.e. 4057 μmol g⁻¹ with 96% selectivity of CO over H₂. The superior catalytic activity is assigned to free Ni atomic sites, keto nodes and the Ni-CO₂ hydrogen-bond reduces the CO₂. Surprisingly despite the reduction of surface area due to the loading of Ni-atoms on TpBpy, Ni-TpBpy captures more CO₂ molecules. This behavior is justified by the Lewis acid-base interaction between CO₂ molecules and loaded Ni-atoms [66].

In based SACs on α-Co(OH)₂ shows faradic efficiency of 97.6% and turnover frequency (TOF) of 38290 h⁻¹ for CO₂RR in aqueous media with current density of 18.6 mA cm⁻². The study indicated that the active



(a)



(b)

Fig. 17. (a) Comparison of common CO₂ electrochemical reduction products and their industrial production conditions [59] (b) Elements explored for CO₂RR electrocatalytic activity; color coding corresponds to product [60,61].

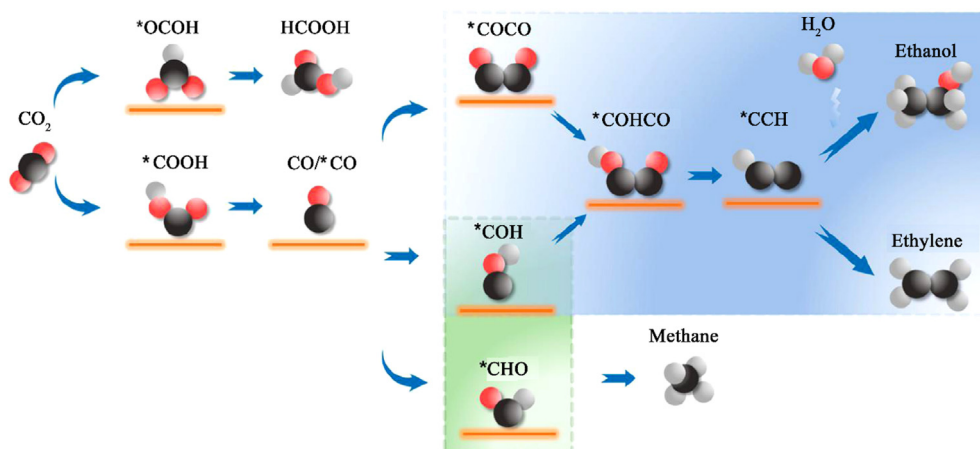


Fig. 18. Cartoon presentation of simplified mechanism and possible reaction pathways for CO₂RR [15].

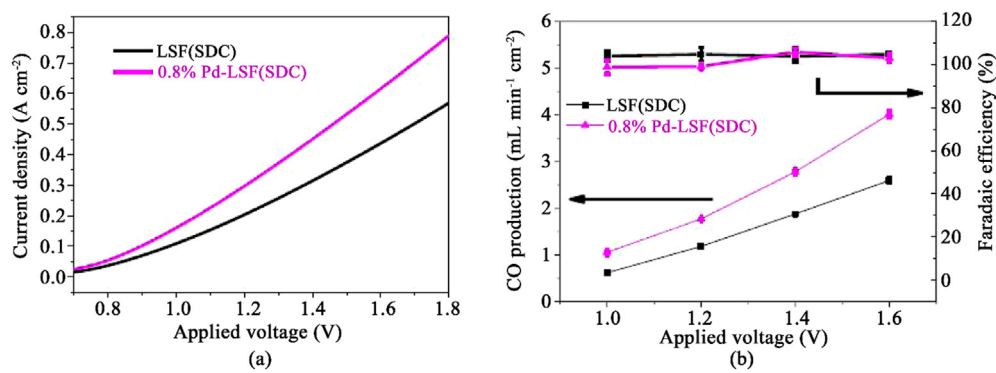


Fig. 19. (left), I-V curves of SOEC for CO₂ electrolysis (top right), CO production rate and Faradaic efficiencies of SOECs with the LSF(SDC) and 0.8% Pd-LSF(SDC) cathode versus applied voltage (bottom right) [57].

surface area for electrochemical reduction is 23.4 times higher as compared to 2 nm Ir nanoparticles, and better conductive. They stabilize the intermediate radical anion (CO₂[•]) which boosts the catalytic activity due to improved electron transfer mechanism. The strong interaction of Ir atoms with support makes this catalyst exceptionally stable [67]. Xuan et al., doped noble metals-based SACs in MoS₂ via electroplating and explored their potential for catalytic activities. Particularly, they synthesized ~7 nm thick MoS₂ two-dimensional (2D) layer on graphite paper electrode and deposited Pd, Pt and Au electrochemically on MoS₂ in a three-electrode cell. Pt–MoS₂ was treated with H₂ plasma to create defects. Presence of Pt single atoms were investigated by TEM showed the line spacing was ~0.62 nm, HAADF-STEM and EDX indicated that Pt atoms were randomly present on the MoS₂ flakes and XRD do not show any crystalline peaks for Pt. MoS₂ has a potential difference (ΔV) of 35 mV with comparison of highly oriented pyrolytic graphite (HOPG) while after Pt atoms doping this value drops to 10 mV measured by Kelvin probe force microscope. XPS confirmed Pt is in +2 oxidation state with binding energies of Pt 4f_{7/2} at 72.1 eV and Pt 4f_{5/2} at 75.5 eV. With single Pt atom the catalyst Pt–2H–MoS₂ was explored for HER and CO₂ reduction reaction into CO with faradic efficiency of 4.56%. The Pt–MoS₂ shows exceptional CO tolerance with almost negligible catalyst poisoning as compared to commercial Pt/C catalyst and stability in performance for 5 h at $\eta = 310$ mV [68]. Zhao and co-workers used DFT calculations to investigate SACs supported on 2D InSe sheets (M@2DInSe, M = V, Cr, Mn, Fe, Co, Ni, Cu, Zn, Ru, Rh, Pd, Ag, Cd, Ir, Pt, and Au). Cr@2DInSe has a limiting potential of -3.6 V and energy profile suggests it is best candidate for CH₄ production. Cu@2DInSe and Mn@2DInSe favors production of HCOOH with limiting potential of -0.11 V and -0.17 V respectively, and Rh favors the formation of H₂. Initial protonation of

CO₂ forms *HCOO which is then converted to *HCOOH, the later step is considered as rate determining step. Their intermediate energy profiles shown in Fig. 20 [69].

Li et al. developed Pt-based SACs supported on MoS₂ for hydrogenation of CO₂ to methanol conversion by synergistic interactions. Pt/MoS₂ catalysts were synthesized by mixing ethanol, water and MoS₂ nanosheets with K₂PtCl₆ solution. Magnified high-angle annular dark-field scanning transmission electron microscopy (HAADF-STEM) revealed that the fraction of Mo atoms was replaced by Pt single atoms or Pt monomers (Fig. 21 a-f). Synergistic effect investigations were carried out with different Pt atomic loadings from 0.2% to 7.5%. Pt mass loading of 15% generates 3 nm small nanoparticles, used for comparison of catalytic and mechanistic studies. XANES studies revealed Pt nanoparticles behaved like Pt foil, hence they stay in the metallic state. In the Pt/MoS₂ the distance between the atomic species decreased with an increase in the atomic concentration of Pt. 0.2% Pt/MoS₂ shows Pt–S shell peak at 2.32 Å and coordination number (CN) 5.2 and no other peaks revealing atomic dispersion. Other samples with different Pt loadings 1.0% Pt/MoS₂, 5.0% Pt/MoS₂ and 7.5% Pt/MoS₂ indicate similar spectra showing that these have atomically dispersed Pt. Nanoparticles/MoS₂ and Pt foil show an additional peak near 2.75 Å for Pt–Pt metallic bond with CN 4.9 (Fig. 21 g-h). The catalytic activity of Pt/MoS₂ was investigated using 32 bar (CO₂:H₂ = 1:3) in DMF. As a control MoS₂ was used and negligible catalytic activity was observed while 0.2% Pt/MoS₂ formic acid (0.003 mmol) and methanol (0.062 mmol) formation occurred at 150 °C and with the increase in temperature at 210 °C the yields increased to 0.4 and 5.7 mmol, respectively. The turnover frequency (TOF) for 7.5% Pt/MoS₂ was highest i.e. 162.5 h⁻¹ which is 14 times higher as compared to 0.2% Pt/MoS₂ [70].

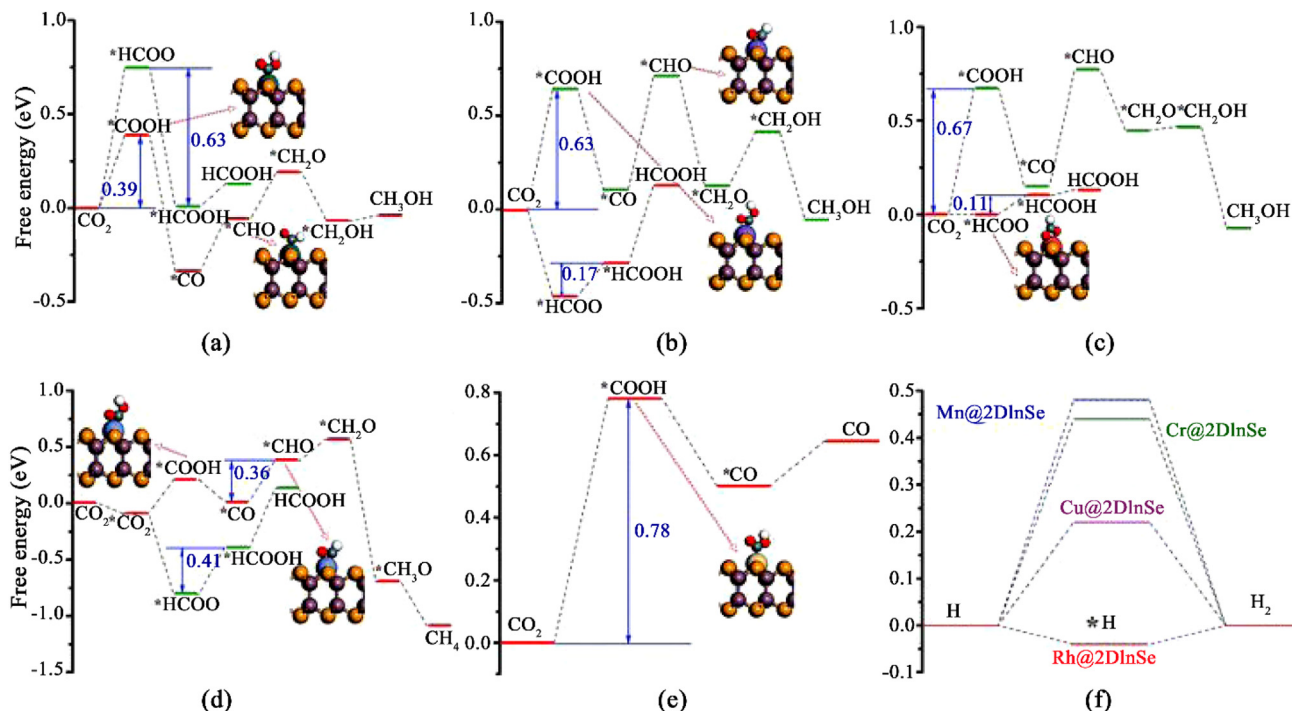


Fig. 20. CO₂RR intermediates free energy profiles for M@2DInSe a) Rh@2DInSe, (b) Mn@2DInSe, (c) Cu@2DInSe, (d) Cr@2DInSe, and (e) Zn@2DInSe and f) for HER for Cu, Cr, Mn and Rh [69].

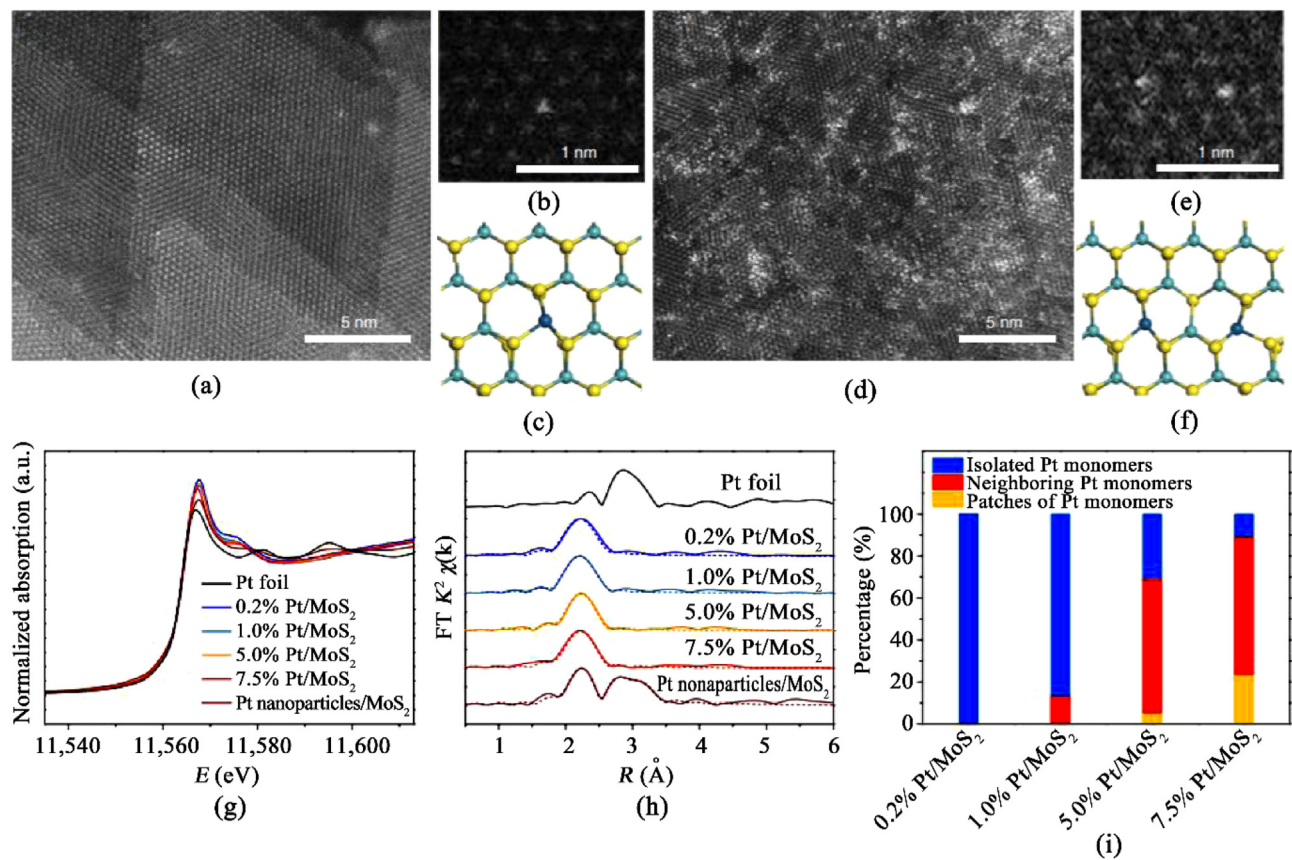


Fig. 21. Pt/MoS₂ characterization a) 0.2% Pt/MoS₂ HAADF-STEM b-c) magnification of HAADF-STEM and correlation structure d) HAADF-STEM of 0.7% Pt/MoS₂ e-f) magnification of HAADF-STEM and correlation structure g) Pt K-edge XANES spectra h) Pt K-edge EXAFS in R space i) Histogram of the contents [70].

4. Summary and outlook

The single atoms easily migrate and are sintered in preparation owing to high surface energy. We can use appropriate support to prevent agglomeration during the sintering of single atoms. So, the single atoms with metal supports are prepared mostly by the wet impregnation method and they are present in the form of isolated species and stabilized on support or they are present in the form of single atoms on the support. By controlling the concentration of loading metal formation of single atoms or the formation of nanoparticles can be controlled and we discussed in details in the synthesis portion of the review.

The single atoms with metal support are thermodynamically more stable as compared to metal alloy or doped materials due to construction of bonds between the isolated species and support. The local configuration makes them more identical than nanoparticles or cluster of same species they are highly active for catalytic applications due to low surface energy and coordination environment. During the electrochemical process, unsaturated coordination environment controls the aggregation of single atoms and make them highly active for specific applications. Furthermore, doped materials face a rapid decline in the catalytic activity due to CO poisoning. They provide lower catalytically active surface area, weaker electronic interaction, and their activity decreased during the harsh electrochemical environment due to leaching of transition. Beyond the physical and chemical stabilities, the single atoms with metal support catalyst provide an extraordinary CO tolerance over the bulk counterpart. The single-atoms with metal support are almost immune to CO poisoning, and their decrease in the activity percentage is negligible. This suggests that stabilized single atoms have fewer free electrons to coordinate with CO. With extraordinary CO tolerance, single-atom with metal oxide support based catalyst has the potential to be utilized in CO-intermediate reactions, such as CO₂RR. During electrocatalysis, bulk materials are poisoned due to the availability of free electrons. This review summarized the diverse design strategies to synthesize single metal atoms on metal oxide supports and structure-activity relationship for CO₂ reduction activity. Further efforts are required for efficient CO₂ reduction catalyst with excellent activity and selectivity for multi-carbon products.

The single atoms catalyst has achieved a number of advances but there are many challenges that need to be addressed. 1) For the industrial and practical applications, it relies on the high density of single atoms with abundant active sites, but the loading of single atoms during the synthesis is significantly low. To fulfil this need a general and large-scale synthetic method with high loading amount of single atoms on the support is required. 2) The electrocatalytic performance of single atoms can be further improved by growing different types of metal single atoms on the same support due to the synergistic effect. 3) The highly surface-sensitive atomic resolution spectroscopic techniques are required to study catalytically active sites because XAFS characterization could only obtain the average information of a whole sample. While single atoms with metal support are coordinated with different N-coordination modes, it is necessary to figure out the true active sites for practical application. 4) The theoretical methods are used to study the structure-activity relationship for electrocatalysis and catalytic mechanisms. However, a big question lies in the poor matching between theoretical and experimental results. Therefore, dynamic behavior and possible structure change during electrocatalysis should be considered in terms of theoretical calculations. It is expected that we can achieve a thorough elucidation of single atom catalysis for practical manipulation for both theoretical and experimental studies.

The biggest challenge for the industrial adoption for CO₂ reduction of promising catalyst is to synthesis catalyst in bulk amount with high selectivity for industrial-scale use. Lack of long-term catalyst stability and complexity of catalyst synthesis are critical factors for not accelerating the commercialization of CO₂ reduction. Few articles unveiled the metal supports for SACs for CO₂RR, for example, Pt SA @FeOx Support, Pt SA@CuS, Pt@CeO₂, Au@CeO₂, Au@TiO₂, and they are used for different application like water gas shift reaction, CO oxidation, selective

oxidation and for coupling reactions, but a very few studies are reported for their catalytic performance for CO₂RR. We combined the present work to give future directions to this field for the preparation of Cu supported single atoms of different metals like Au, Ag, Sn, and Cu based single atoms with different metal support like Au, Ag etc., should be synthesized for CO₂RR. Moreover, these metal support catalyst beds may serve as robust catalysts in comparison with traditional catalysts and nanoparticles that suffer catalyst leaching due to poor stability. These catalysts may exhibit performance metrics of industrial impact.

Declaration of competing interest

The authors declare no conflict of interest.

Acknowledgments

This work was supported by China Postdoctoral Science Foundation under project number 2019M663054.

References

- [1] N. You, S. Cao, M. Huang, X. Fan, K. Shi, H. Huang, Z. Chen, Z. Yang, W. Zhang, Constructing P-CoMoO₄@NiCoP heterostructure nanoarrays on Ni foam as efficient bifunctional electrocatalysts for overall water splitting, *Nano Materials Science* (2021), <https://doi.org/10.1016/j.nanoms.2021.05.004>.
- [2] Z. Zhang, K. Chen, Q. Zhao, M. Huang, X. Ouyang, Electrocatalytic and photocatalytic performance of noble metal doped monolayer MoS₂ in the hydrogen evolution reaction: a first principles study, *Nano Materials Science* 3 (2021) 89–94.
- [3] P. Zhang, W. Xiong, M. Zhou, Effect of nickel oxide morphology on the nitrogen electrochemical reduction reaction, *Nano Materials Science* 2 (2020) 353–359.
- [4] J. Zhang, M. Li, H.A. Younus, B. Wang, Q. Weng, Y. Zhang, S. Zhang, An overview of the characteristics of advanced binders for high-performance Li–S batteries, *Nano Materials Science* 3 (2021) 124–139.
- [5] S.N.A. Haji Yassin, A.S.L. Sim, J.R. Jennings, Photoelectrochemical evaluation of SILAR-deposited nanoporous BiVO₄ photoanodes for solar-driven water splitting, *Nano Materials Science* 2 (2020) 227–234.
- [6] J.G. Canadell, C. Le Quéré, M.R. Raupach, C.B. Field, E.T. Buitenhuis, P. Ciais, T.J. Conway, N.P. Gillett, R.A. Houghton, G. Marland, Contributions to accelerating atmospheric CO₂ growth from economic activity, carbon intensity, and efficiency of natural sinks, *Proc. Natl. Acad. Sci. U.S.A.* 104 (2007) 18866–18870.
- [7] Q. Wang, Y. Liu, G. Zhu, C. Tang, W. Sun, A. Du, M. Wu, H. Zhang, Sn₂₊-Regulated synthesis of a bone-like Fe3O4@N-doped carbon composite as the anode for high-performance lithium storage, *ACS Appl. Energy Mater.* (2021), <https://doi.org/10.1021/acsaelm.1c00189>.
- [8] C. Xu, X. Zhi, A. Vasileff, D. Wang, B. Jin, Y. Jiao, Y. Zheng, S.-Z. Qiao, Highly selective two-electron electrocatalytic CO₂ reduction on single-atom Cu catalysts, *Small. Structures.* 2 (2021), 2000058.
- [9] Q. Yi, W. Li, J. Feng, K. Xie, Carbon cycle in advanced coal chemical engineering, *Chem. Soc. Rev.* 44 (2015) 5409–5445.
- [10] S.A. Mahyoub, A. Hezam, F.A. Qaraah, K. Namratha, M.B. Nayyan, Q.A. Drmosh, D. Ponnamma, K. Byrappa, Surface plasmonic resonance and Z-scheme charge transport synergy in three-dimensional flower-like Ag–CeO₂–ZnO heterostructures for highly improved photocatalytic CO₂ reduction, *ACS Appl. Energy Mater.* (2021), <https://doi.org/10.1021/acsaelm.1c00001>.
- [11] P. Chen, Y. Zhang, Y. Zhou, F. Dong, Photoelectrocatalytic carbon dioxide reduction: fundamental, advances and challenges, *Nano Materials Science* (2021), <https://doi.org/10.1016/j.nanoms.2021.05.003>.
- [12] X. Chen, X. Su, H.-Y. Su, X. Liu, S. Miao, Y. Zhao, K. Sun, Y. Huang, T. Zhang, Theoretical insights and the corresponding construction of supported metal catalysts for highly selective CO₂ to CO conversion, *ACS Catal.* 7 (2017) 4613–4620.
- [13] X. Chang, T. Wang, J. Gong, CO₂ photo-reduction: insights into CO₂ activation and reaction on surfaces of photocatalysts, *Energy Environ. Sci.* 9 (2016) 2177–2196.
- [14] D. Yang, B. Ni, X. Wang, Heterogeneous catalysts with well-defined active metal sites toward CO₂ electrocatalytic reduction, *Adv. Energy Mater.* 10 (2020) 2001142.
- [15] C. Yang, Y. Wang, L. Qian, A.M. Al-Enizi, L. Zhang, G. Zheng, Heterogeneous electrocatalysts for CO₂ reduction, *ACS Appl. Energy Mater.* 4 (2021) 1034–1044.
- [16] S. Ji, Y. Chen, X. Wang, Z. Zhang, D. Wang, Y. Li, Chemical synthesis of single atomic site catalysts, *Chem. Rev.* 120 (2020) 11900–11955.
- [17] Y. Wang, H. Arandiyani, J. Scott, K.-F. Aguey-Zinsou, R. Amal, Single atom and nanoclustered Pt catalysts for selective CO₂ reduction, *ACS Appl. Energy Mater.* 1 (2018) 6781–6789.
- [18] Y. Liu, Z. Li, Q. Yu, Y. Chen, Z. Chai, G. Zhao, S. Liu, W.-C. Cheong, Y. Pan, Q. Zhang, L. Gu, L. Zheng, Y. Wang, Y. Lu, D. Wang, C. Chen, Q. Peng, Y. Liu, L. Liu, J. Chen, Y. Li, A general strategy for fabricating isolated single metal atomic site catalysts in Y zeolite, *J. Am. Chem. Soc.* 141 (2019) 9305–9311.
- [19] C. Li, M. Luo, Z. Xia, S. Guo, High-index faceted noble metal nanostructures drive renewable energy electrocatalysis, *Nano Materials Science* 2 (2020) 309–315.
- [20] J. Liu, Catalysis by supported single metal atoms, *ACS Catal.* 7 (2017) 34–59.

- [21] X.-F. Yang, A. Wang, B. Qiao, J. Li, J. Liu, T. Zhang, Single-atom catalysts: a new frontier in heterogeneous catalysis, *Acc. Chem. Res.* 46 (2013) 1740–1748.
- [22] S.J. Tauster, S.C. Fung, R.L. Garten, Strong metal-support interactions. Group 8 noble metals supported on titanium dioxide, *J. Am. Chem. Soc.* 100 (1978) 170–175.
- [23] N. Acerbi, S.C.E. Tsang, G. Jones, S. Golunski, P. Collier, Rationalization of interactions in precious metal/ceria catalysts using the d-band center model, *Angew. Chem. Int. Ed.* 52 (2013) 7737–7741.
- [24] C.T. Campbell, Electronic perturbations, *Nat. Chem.* 4 (2012) 597–598.
- [25] S.A. Abbas, J.T. Song, Y.C. Tan, K.M. Nam, J. Oh, K.-D. Jung, Synthesis of a nickel single-atom catalyst based on Ni-N4-xC active sites for highly efficient CO₂ reduction utilizing a gas diffusion electrode, *ACS Appl. Energy Mater.* 3 (2020) 8739–8745.
- [26] F. Li, S. Hong, T.-S. Wu, X. Li, J. Masa, Y.-L. Soo, Z. Sun, Atomically dispersed nickel sites for selective electroreduction of CO₂, *ACS Appl. Energy Mater.* 2 (2019) 8836–8842.
- [27] W.E. Kaden, T. Wu, W.A. Kunkel, S.L. Anderson, Electronic structure controls reactivity of size-selected Pd clusters adsorbed on TiO₂ surfaces, *Science* 326 (2009) 826–829.
- [28] P. Hu, Z. Huang, Z. Amghouz, M. Makkee, F. Xu, F. Kapteijn, A. Dikhtiarek, Y. Chen, X. Gu, X. Tang, Electronic metal-support interactions in single-atom catalysts, *Angew. Chem. Int. Ed.* 53 (2014) 3418–3421.
- [29] S. Zhang, J. Li, E. Wang, Recent progress of ruthenium-based nanomaterials for electrochemical hydrogen evolution, *ChemElectroChem* 7 (2020) 4526–4534.
- [30] S. Zhao, R. Jin, R. Jin, Opportunities and challenges in CO₂ reduction by gold- and silver-based electrocatalysts: from bulk metals to nanoparticles and atomically precise nanoclusters, *ACS Energy Lett.* 3 (2018) 452–462.
- [31] X. Li, S. Xi, L. Sun, S. Dou, Z. Huang, T. Su, X. Wang, Isolated FeN4 sites for efficient electrocatalytic CO₂ reduction, *Adv. Sci.* 7 (2020) 2001545.
- [32] R. Lang, X. Du, Y. Huang, X. Jiang, Q. Zhang, Y. Guo, K. Liu, B. Qiao, A. Wang, T. Zhang, Single-atom catalysts based on the metal–oxide interaction, *Chem. Rev.* 120 (2020) 11986–12043.
- [33] B. Qiao, A. Wang, X. Yang, L.F. Allard, Z. Jiang, Y. Cui, J. Liu, J. Li, T. Zhang, Single-atom catalysis of CO oxidation using Pt1/FeOx, *Nat. Chem.* 3 (2011) 634–641.
- [34] R. Lang, W. Xi, J.-C. Liu, Y.-T. Cui, T. Li, A.F. Lee, F. Chen, Y. Chen, L. Li, L. Li, J. Lin, S. Miao, X. Liu, A.-Q. Wang, X. Wang, J. Luo, B. Qiao, J. Li, T. Zhang, Non defect-stabilized thermally stable single-atom catalyst, *Nat. Commun.* 10 (2019) 234.
- [35] T. Wang, J.-Y. Xing, A.-P. Jia, C. Tang, Y.-J. Wang, M.-F. Luo, J.-Q. Lu, CO oxidation over Pt/Cr1.3Fe0.7O3 catalysts: enhanced activity on single Pt atom by H₂O promotion, *J. Catal.* 382 (2020) 192–203.
- [36] R. Shen, W. Chen, Q. Peng, S. Lu, L. Zheng, X. Cao, Y. Wang, W. Zhu, J. Zhang, Z. Zhuang, C. Chen, D. Wang, Y. Li, High-concentration single atomic Pt sites on hollow Cu₃S for selective O₂ reduction to H₂O₂ in acid solution, *Inside Chem.* 5 (2019) 2099–2110.
- [37] J. Zhang, X. Wu, W.-C. Cheong, W. Chen, R. Lin, J. Li, L. Zheng, W. Yan, L. Gu, C. Chen, Q. Peng, D. Wang, Y. Li, Cation vacancy stabilization of single-atomic-site Pt1/Ni(OH)x catalyst for doration of alkynes and alkenes, *Nat. Commun.* 9 (2018) 1002.
- [38] B. Han, Y. Guo, Y. Huang, W. Xi, J. Xu, J. Luo, H. Qi, Y. Ren, X. Liu, B. Qiao, T. Zhang, Strong metal-support interactions between Pt single atoms and TiO₂, *Angew. Chem. Int. Ed.* 59 (2020) 11824–11829.
- [39] S. Hoang, Y. Guo, A.J. Binder, W. Tang, S. Wang, J. Liu, H. Tran, X. Lu, Y. Wang, Y. Ding, E.A. Kyriakidou, J. Yang, T.J. Toops, T.R. Pauly, R. Ramprasad, P.-X. Gao, Activating low-temperature diesel oxidation by single-atom Pt on TiO₂ nanowire array, *Nat. Commun.* 11 (2020) 1062.
- [40] T. Xu, H. Zhao, H. Zheng, P. Zhang, Atomically Pt implanted nanoporous TiO₂ film for photocatalytic degradation of trace organic pollutants in water, *Chem. Eng. J.* 385 (2020) 123832.
- [41] Y. Chen, S. Ji, W. Sun, Y. Lei, Q. Wang, A. Li, W. Chen, G. Zhou, Z. Zhang, Y. Wang, L. Zheng, Q. Zhang, L. Gu, X. Han, D. Wang, Y. Li, Engineering the atomic interface with single platinum atoms for enhanced photocatalytic hydrogen production, *Angew. Chem. Int. Ed.* 59 (2020) 1295–1301.
- [42] M. Moses-DeBusk, M. Yoon, L.F. Allard, D.R. Mullins, Z. Wu, X. Yang, G. Veith, G.M. Stocks, C.K. Narula, CO oxidation on supported single Pt atoms: experimental and ab initio density functional studies of CO interaction with Pt atom on 0-Al2O3(010) surface, *J. Am. Chem. Soc.* 135 (2013) 12634–12645.
- [43] J. Xu, C. Zhang, H. Liu, J. Sun, R. Xie, Y. Qiu, F. Lü, Y. Liu, L. Zhuo, X. Liu, J. Luo, Amorphous MoOX-Stabilized single platinum atoms with ultrahigh mass activity for acidic hydrogen evolution, *Nanomater. Energy* 70 (2020) 104529.
- [44] X. Pan, S. Lu, D. Zhang, Y. Zhang, F. Duan, H. Zhu, H. Gu, S. Wang, M. Du, Atom-precise incorporation of platinum into ultrafine transition metal carbides for efficient synergistic electrochemical hydrogen evolution, *J. Mater. Chem.* 8 (2020) 4911–4919.
- [45] H. Shin, W.-G. Jung, D.-H. Kim, J.-S. Jang, Y.H. Kim, W.-T. Koo, J. Bae, C. Park, S.-H. Cho, B.J. Kim, I.-D. Kim, Single-atom Pt stabilized on one-dimensional nanostructure support via carbon nitride/SnO₂ heterojunction trapping, *ACS Nano* 14 (2020) 11394–11405.
- [46] C. Wang, S. Mao, Z. Wang, Y. Chen, W. Yuan, Y. Ou, H. Zhang, Y. Gong, Y. Wang, B. Mei, Z. Jiang, Y. Wang, Insight into single-atom-induced unconventional size dependence over CeO₂-supported Pt catalysts, *Inside Chem.* 6 (2020) 752–765.
- [47] L. Kuai, Z. Chen, S. Liu, E. Kan, N. Yu, Y. Ren, C. Fang, X. Li, Y. Li, B. Geng, Titania supported synergistic palladium single atoms and nanoparticles for room temperature ketone and aldehydes hydrogenation, *Nat. Commun.* 11 (2020) 48.
- [48] X. Ge, P. Zhou, Q. Zhang, Z. Xia, S. Chen, P. Gao, Z. Zhang, L. Gu, S. Guo, Palladium single atoms on TiO₂ as a photocatalytic sensing platform for analyzing the organophosphorus pesticide chlorpyrifos, *Angew. Chem. Int. Ed.* 59 (2020) 232–236.
- [49] J. Lin, A. Wang, B. Qiao, X. Liu, X. Yang, X. Wang, J. Liang, J. Li, J. Liu, T. Zhang, Remarkable performance of Ir1/FeOx single-atom catalyst in water gas shift reaction, *J. Am. Chem. Soc.* 135 (2013) 15314–15317.
- [50] Q. Wang, X. Huang, Z.L. Zhao, M. Wang, B. Xiang, J. Li, Z. Feng, H. Xu, M. Gu, Ultrahigh-loading of Ir single atoms on NiO matrix to dramatically enhance oxygen evolution reaction, *J. Am. Chem. Soc.* 142 (2020) 7425–7433.
- [51] S. Tian, W. Gong, W. Chen, N. Lin, Y. Zhu, Q. Feng, Q. Xu, Q. Fu, C. Chen, J. Luo, W. Yan, H. Zhao, D. Wang, Y. Li, Regulating the catalytic performance of single-atomic-site Ir catalyst for biomass conversion by metal-support interactions, *ACS Catal.* 9 (2019) 5223–5230.
- [52] K. Liu, X. Zhao, G. Ren, T. Yang, Y. Ren, A.F. Lee, Y. Su, X. Pan, J. Zhang, Z. Chen, J. Yang, X. Liu, T. Zhou, W. Xi, J. Luo, C. Zeng, H. Matsumoto, W. Liu, Q. Jiang, K. Wilson, A. Wang, B. Qiao, W. Li, T. Zhang, Strong metal-support interaction promoted scalable production of thermally stable single-atom catalysts, *Nat. Commun.* 11 (2020) 1263.
- [53] Q. He, D. Tian, H. Jiang, D. Cao, S. Wei, D. Liu, P. Song, Y. Lin, L. Song, Achieving efficient alkaline hydrogen evolution reaction over a Ni5P4 catalyst incorporating single-atomic Ru sites, *Adv. Mater.* 32 (2020) 1906972.
- [54] Z. Kou, W. Zang, W. Pei, L. Zheng, S. Zhou, S. Zhang, L. Zhang, J. Wang, A sacrificial Zn strategy enables anchoring of metal single atoms on the exposed surface of holey 2D molybdenum carbide nanosheets for efficient electrocatalysis, *J. Mater. Chem.* 8 (2020) 3071–3082.
- [55] M. Xiao, L. Zhang, B. Luo, M. Lyu, Z. Wang, H. Huang, S. Wang, A. Du, L. Wang, Molten-salt-mediated synthesis of an atomic nickel Co-catalyst on TiO₂ for improved photocatalytic H₂ evolution, *Angew. Chem. Int. Ed.* 59 (2020) 7230–7234.
- [56] Y. Wang, Z. Chen, P. Han, Y. Du, Z. Gu, X. Xu, G. Zheng, Single-atomic Cu with multiple oxygen vacancies on ceria for electrocatalytic CO₂ reduction to CH₄, *ACS Catal.* 8 (2018) 7113–7119.
- [57] Y. Zhou, L. Lin, Y. Song, X. Zhang, H. Lv, Q. Liu, Z. Zhou, N. Ta, G. Wang, X. Bao, Pd single site-anchored perovskite cathode for CO₂ electrolysis in solid oxide electrolysis cells, *Nanomater. Energy* 71 (2020) 104598.
- [58] S.I.O. Oceanography, in: N.a.S.I.O. Oceanography (Ed.), *Rise of Carbon Dioxide Unabated*, 2020.
- [59] S. Verma, S. Lu, P.J.A. Kenis, Co-electrolysis of CO₂ and glycerol as a pathway to carbon chemicals with improved technoeconomics due to low electricity consumption, *Nature Energy* 4 (2019) 466–474.
- [60] M. Li, H. Wang, W. Luo, P.C. Sherrell, J. Chen, J. Yang, Heterogeneous single-atom catalysts for electrochemical CO₂ reduction reaction, *Adv. Mater.* 32 (2020) 2001848.
- [61] A.S. Varela, W. Ju, A. Bagger, P. Franco, J. Rossmeisl, P. Strasser, Electrochemical reduction of CO₂ on metal-nitrogen-doped carbon catalysts, *ACS Catal.* 9 (2019) 7270–7284.
- [62] G. Xing, L. Cheng, K. Li, Y. Gao, H. Tang, Y. Wang, Z. Wu, Efficient electroreduction of CO₂ by single-atom catalysts two-dimensional metal hexahydroxybenzene frameworks: a theoretical study, *Appl. Surf. Sci.* 550 (2021) 149389.
- [63] J. Gu, C.-S. Hsu, L. Bai, H.M. Chen, X. Hu, Atomically dispersed Fe³⁺ sites catalyze efficient CO₂ electroreduction to CO, *Science* 364 (2019) 1091–1094.
- [64] H. Yang, Y. Wu, G. Li, Q. Lin, Q. Hu, Q. Zhang, J. Liu, C. He, Scalable production of efficient single-atom copper decorated carbon membranes for CO₂ electroreduction to methanol, *J. Am. Chem. Soc.* 141 (2019) 12717–12723.
- [65] T. Zheng, K. Jiang, N. Ta, Y. Hu, J. Zeng, J. Liu, H. Wang, Large-scale and highly selective CO₂ electrocatalytic reduction on nickel single-atom catalyst, *Joule* 3 (2019) 265–278.
- [66] W. Zhong, R. Sa, L. Li, Y. He, L. Li, J. Bi, Z. Zhuang, Y. Yu, Z. Zou, A covalent organic framework bearing single Ni sites as a synergistic photocatalyst for selective photoreduction of CO₂ to CO, *J. Am. Chem. Soc.* 141 (2019) 7615–7621.
- [67] X. Sun, C. Chen, S. Liu, S. Hong, Q. Zhu, Q. Qian, B. Han, J. Zhang, L. Zheng, Aqueous CO₂ reduction with high efficiency using α-Co(OH)₂-Supported atomic Ir electrocatalysts, *Angew. Chem. Int. Ed.* 58 (2019) 4669–4673.
- [68] N. Xuan, J. Chen, J. Shi, Y. Yue, P. Zhuang, K. Ba, Y. Sun, J. Shen, Y. Liu, B. Ge, Z. Sun, Single-atom electroplating on two dimensional materials, *Chem. Mater.* 31 (2019) 429–435.
- [69] C.-X. Zhao, G.-X. Zhang, W. Gao, Q. Jiang, Single metal atoms regulated flexibly by a 2D InSe substrate for CO₂ reduction electrocatalysts, *J. Mater. Chem.* 7 (2019) 8210–8217.
- [70] H. Li, L. Wang, Y. Dai, Z. Pu, Z. Lao, Y. Chen, M. Wang, X. Zheng, J. Zhu, W. Zhang, R. Si, C. Ma, J. Zeng, Synergetic interaction between neighbouring platinum monomers in CO₂ hydrogenation, *Nat. Nanotechnol.* 13 (2018) 411–417.
- [71] S.A. Mahyoub, A. Hezam, F.A. Qaraah, K. Namratha, M.B. Nayyan, Q.A. Drmoh, D. Ponnamma, K. Byrappa, Surface plasmonic resonance and Z-scheme charge transport synergy in three-dimensional flower-like Ag–CeO₂–ZnO heterostructures for highly improved photocatalytic CO₂ reduction, *ACS Appl. Energy Mater.* 4 (2021) 3544–3554.